

**UNIVERSIDADE FEDERAL DE JUIZ DE FORA**  
**INSTITUTO DE CIÊNCIAS EXATAS**  
**PROGRAMA DE PÓS-GRADUAÇÃO EM MODELAGEM COMPUTACIONAL**

**Gilmar Ferreira da Silva Filho**

**Forward Uncertainty Quantification and Sensitivity Analysis in Models of Systemic  
Circulation**

Juiz de Fora

2020



**Gilmar Ferreira da Silva Filho**

**Forward Uncertainty Quantification and Sensitivity Analysis in Models of Systemic Circulation**

Dissertação apresentada ao Programa de Pós-Graduação em Modelagem Computacional da Universidade Federal de Juiz de Fora como requisito parcial à obtenção do título de Mestre em Modelagem Computacional.

Orientador: Prof. D.Sc. Bernardo Martins Rocha

Coorientador: Prof. D.Sc. Luis Paulo da Silva Barra

Coorientador: Prof. D.Sc. Rafael Alves Bofim de Queiroz

Juiz de Fora

2020

Ficha catalográfica elaborada através do programa de geração automática da Biblioteca Universitária da UFJF, com os dados fornecidos pelo(a) autor(a)

Silva Filho, Gilmar Ferreira da.

Forward uncertainty quantification and sensitivity analysis in models of systemic circulation / Gilmar Ferreira da Silva Filho. -- 2020.

86 p. : il.

Orientador: Bernardo Martins Rocha

Coorientadores: Luis Paulo da Silva Barra, Rafael Alves Bonfim de Queiroz

Dissertação (mestrado acadêmico) - Universidade Federal de Juiz de Fora, Instituto de Ciências Exatas. Programa de Pós-Graduação em Modelagem Computacional, 2020.

1. Quantificação de incertezas. 2. Análise de sensibilidade. 3. Modelagem cardiovascular. 4. Modelos de parâmetros condensados. 5. Caos polinomial. I. Rocha, Bernardo Martins, orient. II. Barra, Luis Paulo da Silva, coorient. III. Queiroz, Rafael Alves Bonfim de, coorient. IV. Título.

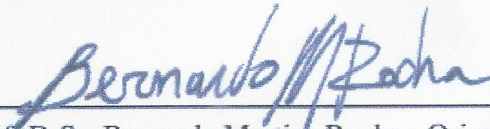
**Gilmar Ferreira da Silva Filho**

**Forward Uncertainty Quantification and Sensitivity Analysis in Models of Systemic Circulation**

Dissertação apresentada ao Programa de Pós-Graduação em Modelagem Computacional da Universidade Federal de Juiz de Fora como requisito parcial à obtenção do título de Mestre em Modelagem Computacional.

Aprovada em 10 de setembro de 2020

**BANCA EXAMINADORA**



---

Prof. D.Sc. Bernardo Martins Rocha - Orientador  
Universidade Federal de Juiz de Fora



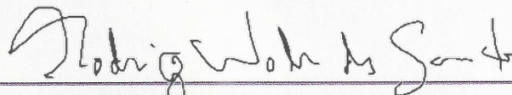
---

Prof. D.Sc. Luis Paulo da Silva Barra - Coorientador  
Universidade Federal de Juiz de Fora



---

Prof. D.Sc. Rafael Alves Bofim de Queiroz - Coorientador  
Universidade Federal de Juiz de Fora



---

Prof. D.Sc. Rodrigo Weber dos Santos  
Universidade Federal de Juiz de Fora



---

Prof. Ph.D. Joakim Sundnes  
Simula School of Research and Innovation



Aos meus familiares e aos que acreditaram em mim.



## **AGRADECIMENTOS**

Agradeço aos meus pais e familiares, pelo apoio e encorajamento. Aos professores Bernardo, Rafael e Luis Paulo pelos ensinamentos, orientação, paciência e amizade. Ao programa de pós-graduação em Modelagem Computacional da Universidade Federal de Juiz de Fora, pelo suporte, estrutura e amizades.



## RESUMO

A intrincada natureza do coração e da circulação sanguínea é intensamente estudada na busca de respostas e *insights* capazes de amadurecer a compreensão dos fenômenos fisiológicos e patofisiológicos do sistema cardiovascular. Modelos computacionais cardiovasculares são ferramentas úteis para este fim e já são amplamente utilizados pela comunidade médico-científica, sendo capazes de simular fenômenos importantes como as dinâmicas da circulação sistêmica e fornecer informações valiosas, como parâmetros hemodinâmicos e biomarcadores, de habitual uso clínico. Entretanto, a aplicação destes modelos em cenários clínicos não se dá facilmente, e para que sejam usados de forma ubíqua para a tomada de decisão ainda há muito o que se aprimorar. Um importante passo neste sentido se dá na busca por modelos mais precisos e confiáveis, onde deve-se tomar em conta o entendimento da relação entre as incertezas nos parâmetros de entrada de um modelo e a precisão de seus resultados. No presente trabalho, verificamos o efeito da propagação de incertezas nos parâmetros de entradas de modelos de parâmetros condensados e um modelo de elementos finitos multi-escala que simulam as dinâmicas da circulação sistêmica. Para isto, realizamos a quantificação de incertezas direta e análise de sensibilidade baseadas na expansão por caos polinomial e os resultados obtidos apontam para os parâmetros mais influentes na predição de quantidades de interesse de relevância clínica. Desta forma, espera-se que os conhecimentos adquiridos sobre os parâmetros que devem ser medidos com maior precisão, bem como os menos influentes, que podem ser medidos a partir de valores de base populacional ou da literatura, possam ajudar na calibragem e desenvolvimento de modelos mais precisos e consistentes.

Palavras-chave: Quantificação de Incertezas. Análise de Sensibilidade. Modelagem Cardiovascular. Modelos de Parâmetros Condensados. Caos Polinomial.



## ABSTRACT

The intricate nature of the heart and blood circulation is intensively studied in the search for answers and insights capable of maturing the understanding of the cardiovascular system's physiological and pathophysiological phenomena. Cardiovascular computational models are useful tools for this purpose. They are already widely used by the medical-scientific community, simulating important phenomena such as the dynamics of the systemic circulation and providing valuable information, such as hemodynamic parameters and biomarkers, of common clinical use. However, the clinical application of these models is not straightforward, and for them to be used ubiquitously for decision-making, there is still much to be improved. An important step in this direction is to search for more accurate and reliable models, where the understanding of the relationship between the uncertainties in the input parameters of a model and the precision of its results must be taken into account. In the present work, we verify the effect of the propagation of uncertainties on the input parameters of lumped parameter models and a multi-scale finite element model that simulates the systemic circulation dynamics. For this, we perform forward uncertainty quantification and sensitivity analysis based on the polynomial chaos expansion. The results obtained point to the most influential parameters in the prediction of quantities of interest of clinical relevance. Thus, it is expected that the knowledge acquired on the parameters that must be measured with greater precision and the least influential ones, which can be measured from population-based values or the literature, can help in the calibration and development of more accurate and consistent models.

**Keywords:** Uncertainty Quantification. Sensitivity Analysis. Cardiovascular Modelling. Lumped Parameter Models. Polynomial Chaos.



## LIST OF FIGURES

Figure 1 – The logistic growth model evaluations. . . . .	36
Figure 2 – Monte Carlo simulation of the logistic growth model. . . . .	36
Figure 3 – Mean value and standard deviation convergence for the Monte Carlo method. 38	
Figure 4 – Schematic diagram of the cardiovascular system circulation . . . . .	40
Figure 5 – Left ventricular pressure-volume loop. . . . .	42
Figure 6 – Cardiac myocyte structure. . . . .	43
Figure 7 – A resistance vessel. . . . .	45
Figure 8 – A compliance vessel. . . . .	46
Figure 9 – Time-varying elastance function. . . . .	47
Figure 10 – Five-compartment model. . . . .	48
Figure 11 – Three-compartment model . . . . .	50
Figure 12 – Five-compartment model simulation . . . . .	53
Figure 13 – Comparison between the simulation of the two models. . . . .	55
Figure 14 – Active stress curve. . . . .	57
Figure 15 – Flowchart of the coupling scheme. . . . .	59
Figure 16 – Coupled model . . . . .	60
Figure 17 – Active stress and elastance curves . . . . .	62
Figure 18 – Coupled model simulation results. . . . .	63
Figure 19 – Left ventricle during the cardiac cycle. . . . .	64
Figure 20 – Uncertainty propagation in the 5-compartment model for the left heart pressure and volume. . . . .	66
Figure 21 – Evaluated distribution of each scalar QoIs for the 5-compartment model. 67	
Figure 22 – Sensitivity analysis for the 5-compartment model. . . . .	68
Figure 23 – Uncertainty propagation in the 3-compartment model for the left ventricular pressure and volume. . . . .	70
Figure 24 – Sensitivity analysis for the 3-compartment model. . . . .	71
Figure 25 – Uncertainty propagation in the coupled model for left ventricular pressure and volume. . . . .	73
Figure 26 – Uncertainty propagation for the LV pressure-volume loop in the coupled model. . . . .	73
Figure 27 – Evaluated distribution of each scalar QoIs for the coupled model. . . .	74
Figure 28 – Sensitivity analysis for the coupled model. . . . .	75



## LIST OF TABLES

Table 1	– UQ and SA results for the logistic growth model: $p$ is the polynomial degree, $m$ the multiplicative factor of the minimum number of samples required $N_s$ , the number of samples used to create the surrogate model, and $Q^2$ is the determination coefficient. . . . .	38
Table 2	– Normal resting pressure ( $P$ ) and volume ( $V$ ) of the systemic and pulmonary vessels. . . . .	40
Table 3	– Normal left ventricular hemodynamic values by age deciles for male and female subjects; Max AP: maximum arterial pressure; Min AP: minimum arterial pressure; CI: confidence interval; SD: standard deviation. . . . .	43
Table 4	– Five-compartment model: initial conditions and parameters. . . . .	52
Table 5	– Hemodynamic values obtained in the simulations of the 5-compartment model. . . . .	53
Table 6	– Three-compartment model: initial conditions and parameters. . . . .	54
Table 7	– Comparison between values obtained in the simulations of the models. . . . .	55
Table 8	– Coupled model: initial conditions and parameters. . . . .	61
Table 9	– Hemodynamic values obtained in the simulations of the coupled. . . . .	63
Table 10	– LOO accuracy for each QoI of the 5-compartment model. . . . .	66
Table 11	– Uncertainty measures of each QoI for the 5-compartment model. . . . .	66
Table 12	– LOO accuracy for each QoI for the 3-compartment model. . . . .	69
Table 13	– Uncertainty measures of each QoI for the 3-compartment model. . . . .	69
Table 14	– Uncertainty measures of each QoI for the coupled model. . . . .	72



## LIST OF ABBREVIATIONS AND ACRONYMS

Ao	Aorta
CI	Confidence Interval
EDV	End-Diastolic Function
EDPVR	End-Diastolic Pressure Volume Relationship
EF	Ejection Fraction
ESV	End-Systolic Function
ESPVR	End-Systolic Pressure Volume Relationship
FE	Finite Element
gPC	generalized Polynomial Chaos
IVC	Inferior Vena Cava
LA	Left Atrium
LP	Lumped Parameter
LV	Left Ventricle
Max AP	Maximum Arterial Pressure
Min AP	Minimum Arterial Pressure
PI	Prediction Interval
RA	Right Atrium
RV	Right Ventricle
PA	Pulmonary Artery
SA	Sensitivity Analysis
SD	Standard Deviation
SV	Stroke Volume
SVC	Superior Vena Cava
UQ	Uncertainty Quantification



## SUMMARY

<b>1</b>	<b>INTRODUCTION</b> . . . . .	<b>21</b>
1.1	OBJECTIVES . . . . .	23
1.2	RELATED WORKS . . . . .	23
1.3	OUTLINE OF THE DISSERTATION . . . . .	24
<b>2</b>	<b>UNCERTAINTY QUANTIFICATION AND SENSITIVITY ANALYSIS</b>	<b>25</b>
2.1	MODELS AND UNCERTAINTY . . . . .	25
2.2	AN OVERVIEW OF UQ AND SA TECHNIQUES . . . . .	26
<b>2.2.1</b>	<b>Input prioritization and input fixing</b> . . . . .	<b>27</b>
2.3	UNCERTAINTY QUANTIFICATION . . . . .	28
2.4	SENSITIVITY ANALYSIS . . . . .	29
<b>2.4.1</b>	<b>Time series sensitivity analysis</b> . . . . .	<b>29</b>
2.5	GENERALIZED POLYNOMIAL CHAOS . . . . .	30
<b>2.5.1</b>	<b>gPC expansion</b> . . . . .	<b>30</b>
<b>2.5.2</b>	<b>Determination of the expansion coefficients</b> . . . . .	<b>31</b>
<b>2.5.3</b>	<b>UQ and SA metrics from the gPC</b> . . . . .	<b>32</b>
2.6	ACCURACY OF THE SURROGATE MODEL . . . . .	33
2.7	THE ChaosPy TOOLBOX . . . . .	34
<b>2.7.1</b>	<b>An illustrative example</b> . . . . .	<b>34</b>
<b>2.7.2</b>	<b>Example of UQ and SA</b> . . . . .	<b>35</b>
<b>3</b>	<b>CARDIOVASCULAR MODELS</b> . . . . .	<b>39</b>
3.1	CARDIOVASCULAR PHYSIOLOGY BACKGROUND . . . . .	39
<b>3.1.1</b>	<b>The cardiac cycle</b> . . . . .	<b>41</b>
<b>3.1.2</b>	<b>Heart contraction</b> . . . . .	<b>43</b>
3.2	LUMPED PARAMETER CIRCULATORY MODELS . . . . .	44
<b>3.2.1</b>	<b>Five-compartment model</b> . . . . .	<b>47</b>
<b>3.2.2</b>	<b>A reduced model</b> . . . . .	<b>49</b>
<b>3.2.3</b>	<b>Numerical solution</b> . . . . .	<b>51</b>
<b>3.2.4</b>	<b>Five-compartment model simulation</b> . . . . .	<b>52</b>
<b>3.2.5</b>	<b>Three-compartment model simulation</b> . . . . .	<b>54</b>
3.3	COUPLED MODEL . . . . .	54
<b>3.3.1</b>	<b>Cardiac tissue mechanics model</b> . . . . .	<b>55</b>
<b>3.3.2</b>	<b>Active stress</b> . . . . .	<b>56</b>
<b>3.3.3</b>	<b>Models coupling</b> . . . . .	<b>57</b>
<b>3.3.4</b>	<b>Numerical solution of the coupled model</b> . . . . .	<b>60</b>
<b>3.3.5</b>	<b>Coupled model simulation</b> . . . . .	<b>60</b>
<b>4</b>	<b>RESULTS</b> . . . . .	<b>65</b>
4.1	ANALYSIS OF THE FIVE-COMPARTMENT MODEL . . . . .	65

4.1.1	<b>UQ and SA results</b>	65
4.2	ANALYSIS OF THREE-COMPARTMENT MODEL	68
4.2.1	<b>UQ and SA results</b>	69
4.3	ANALYSIS OF THE COUPLED MODEL	70
4.3.1	<b>UQ and SA results</b>	72
4.4	DISCUSSION	73
4.4.1	<b>Lumped parameter models</b>	74
4.4.1.1	<i>Model reduction</i>	75
4.4.2	<b>Coupled model</b>	76
4.4.3	<b>Related work</b>	77
5	<b>CONCLUSION</b>	<b>79</b>
5.1	LIMITATIONS AND FUTURE WORKS	79
	<b>REFERENCES</b>	<b>81</b>

## 1 INTRODUCTION

Annually, more people die in the world from cardiovascular disease than from any other disease. Cardiovascular diseases killed approximately 17.9 million people in 2016, representing 31% of all deaths in the world (1). In Brazil, approximately 45.7 million people over the age of 20 suffer from heart failure, myocardial infarction, atrial fibrillation, or hypertension, representing around 32% of the entire adult population. The financial cost that these diseases entailed for Brazil in 2015 results in approximately R\$ 56.2 billion, which represents 5.5% of the total national expenditure on health care (2).

It is known that many cardiovascular complications can be prevented as long as attention is paid to risky behaviors such as the use of tobacco and alcohol, unhealthy diet or lack of physical activities (1). Nevertheless, ethical and practical limitations constitute a major obstacle to a better understanding of the complex mechanisms inherent to the cardiovascular system and its pathologies. They make it difficult to obtain more detailed information in experimental and clinical settings (3, 4).

However, a promising alternative to conventional empirical medicine is to take advantage of advances in obtaining increasingly detailed diagnostic data and integrate them with physical and mathematical principles to build robust computational models. The models are used to simulate the specific reality of a patient and, consequently, can provide a platform that enables the study of complex physiological phenomena such as the cardiac mechanics (5), cardiac electrophysiology (6), or blood flow dynamics (7). Predictions arising from these models bring up relevant questions and answers for the best understanding of the cardiovascular system in healthy and pathological scenarios (8, 9).

In the literature, many studies already consider cardiovascular patient-specific modeling. There are works considering: the patient-specific simulation of blood flow in the abdominal aorta (10), pressure and flow in the arterial system in conditions of rest and light exercise (11), effects of geometric changes arising from the process of surgical restoration of the ventricle (12), response to cardiac resynchronization therapy (13), mechanisms of micro-reentries that generate ectopic beats close to areas of infarction (14), and many others (8, 9).

Models of the cardiovascular physiology can provide fundamental information ranging from the cellular level to muscle tissue level (15, 16, 17). In particular, information related to cardiovascular hemodynamics is essential in clinical settings, since they can be used to obtain essential physiological measures and biomarkers of high relevance for treatment and therapy design (7, 18). These hemodynamic measures can be obtained using both simpler lumped parameter (LP) models (19) and advanced multi-scale models that combine cardiovascular hemodynamics, electrophysiology, and mechanics (20).

Through a representation analogous to electrical circuits, LP models are designed to represent the cardiovascular dynamics. They can be as simple as a three-compartment (or

3-compartment) windkessel model of the arterial system (19), and as complex as a model for the global hemodynamics with over 153 parameters (21). Thanks to their capability of representing the cardiovascular dynamics under various physiological and pathological conditions, the simulations of LP models find many clinical and patient-specific uses (22, 23, 24, 25). However, some of these models, especially the most complex ones, are commonly developed for research purposes only (18).

On the other hand, LP models are especially useful to obtain more realistic and detailed representations of multi-scale simulations predictions (7, 5, 18). They can model the cardiovascular hemodynamics to provide correct boundary conditions when coupled with more complex and higher-dimensional models of local cardiovascular elements, such as the ventricles and the atria or the coronary arteries (26, 27, 11). Many of the patient-specific works already mentioned use LP models to this end (27, 11, 13, 10).

Nonetheless, in a clinical context, where patient-specific complexities are relevant, the greatest challenge is to achieve a model that accurately describes the patient's personal reality with a reasonable level of complexity (28). One way to capture patient-specific information to serve as model inputs is by calibrating model parameters aided by measured observations. However, most of the time, clinical data are inevitably hampered with measurement uncertainties and insufficient to provide all the necessary input parameters for a model. Physiological properties vary considerably between subjects, leading to a tremendous source of variability in the model parameters (29). Thus, a better understanding of the model behavior is necessary to increase its robustness and accuracy. Great insights into the model functioning can be achieved through uncertainty quantification (UQ) of model predictions. Forward UQ analysis can be used to study how the measurement errors propagate from input parameters to the model predictions and is usually evaluated by means of useful metrics such as statistical moments, percentiles, and confidence intervals. Besides, the investigation of the model can be improved by a detailed sensitivity analysis (SA), which is useful to find out which uncertain inputs are responsible for more variations in the outputs.

Several works have considered the application of UQ and SA methods to study the effects of uncertainties on the simulation of cardiovascular hemodynamics (28, 30, 31, 4, 32, 33). Most of them analyze by using the so-called local methods (34, 35), which consist in verifying the effects on the output caused by local variations around the baseline value of one input parameter while keeping all other inputs fixed. Very few of them account for uncertainties on the whole input domain and the interactions between inputs (3), which is done through global methods (34, 35). Since they make no assumptions about linearity, additivity, or monotonicity, global methods are considered gold standard practice for UQ and SA (36). There are several global methods, but one of the most used methods is the generalized polynomial chaos (gPC). Proposed as a generalization of the classical polynomial chaos (37) by (38), it stands out for its remarkable precision and efficiency.

## 1.1 OBJECTIVES

This work presents a proof of concept study on UQ and SA methods for the investigation and simplification of mathematical models of cardiovascular circulation. We seek to verify how uncertainties on parameters of mathematical models of the systemic circulation can impact model predictions of essential biomarkers. We will focus on using forward UQ and SA methods to determine which parameters are most influential, and therefore, more rewarding to be measured with higher precision (input prioritization). Also, we investigate which parameters have a negligible influence on the outputs of interest to be fixed to population-based or literature values (input fixing).

We apply the gPC method to perform global UQ and SA on the simulation of a complete cardiac cycle with a five-compartment (or 5-compartment) LP model of the systemic circulation. We then study a reduced version of the model with only three compartments and perform the same analyses in this model. Finally, we couple the resulting three-compartment model to a left ventricular finite element (FE) model to achieve a multi-scale model. Then, we study the effects of uncertainties on input parameters related to the left ventricle's mechanical function during a whole cardiac cycle. We hope to show that the information acquired with this study can help grasp the models' overall performance and provide useful insights into model calibration, simplification, and enhancement.

## 1.2 RELATED WORKS

In the context of cardiovascular modeling, some recent studies seek to analyze and quantify the uncertainties in the model input data so that the predictions become increasingly accurate and robust, capable of capturing the biological variability of each individual.

In the study of (30), the sensitivity of parameters for an 11-compartment model developed to understand the dynamics of cerebral blood flow velocity and finger blood pressure during a postural change from sitting to standing was studied. They used local sensitivity analysis data to predict 22 of 52 parameters for a single dataset accurately and design a reduced model that retained the original model features. An automated framework for tuning of LP model parameters based on local identifiability and inverse Bayesian parameter estimation was presented in the work of (39). Another recent study by (32) applied inverse UQ methods to estimate parameters and prediction intervals for a LP model considering experimental data for rats. In the work of (33), local SA were used to study pulsatile and non-pulsatile models for the cardiovascular dynamics during head-up tilt protocol (HUT), which is often used to diagnose pathologies in the autonomic control system.

In this context of cardiovascular modeling, the number of works that apply global UQ and SA is still small (3). The work of (28) analyzed the effects of uncertainties in arterial wall

model parameters on the predictions of pressure and flow waves in an arterial network. They used the gPC approach to estimate the sensitivity metrics for quantities such as the wave speed and cross-sectional area. They also proposed the time series sensitivity indices to assess the pressure and flow time series. The study of (31) analyzed the influence of parameters in the calculation of measures such as the mean brachial flow and systolic radial artery pressure after the arteriovenous fistula surgery in six different patients. Applying a variance-based SA through a Monte Carlo approach, they identified influential parameters of an LP pulse wave propagation model. Their findings showed that 16 parameters importantly influence the outputs of interest, while 51 out of 73 parameters could be fixed within their measurement uncertainties.

There are also studies regarding uncertainties in multi-scale models of cardiovascular dynamics. In (4) they considered the effects of mechanical and circulatory parameters on the measuring of clinically-relevant circulatory and mechanical quantities, such as the EF and the ventricular wall thickness, through the simulation of a strongly-coupled electromechanical model. Applying local and global sampling-based methods, they have shown that significant variations on parameters such as vessel compliances and the maximum active stress value can lead to considerable variability in mechanical biomarkers, ranging from healthy to diseased values. However, many studies of multi-scale models focus on the propagation of uncertainties to measures related to the heart's electromechanical behavior. Some of these works regard parametric uncertainties on the simulation of ventricular electrophysiology to measure the action potential of ventricular cell (40, 41). Other works consider the mechanical function of the heart and analyze the effects of uncertainties in parameters for the fiber orientation, wall thickness, and constitutive laws of ventricular tissue (15, 42, 43).

### 1.3 OUTLINE OF THE DISSERTATION

This text is organized into five chapters, where all the concepts, methods, results, and concluding remarks are presented. In the second chapter UQ and SA methods are described together with an overview of this field of study. The third chapter, introduces the fundamental concepts of the cardiovascular physiology necessary to subsequently discuss the methods regarded to implement and numerically solve the models studied. The fourth chapter presents the results obtained for all the experiments performed in this work. The UQ and SA results are presented first for the 5-compartment model, then for the 3-compartment model, and lastly for the coupled model. It closes with a discussion of the main findings of the experiments. The fifth chapter presents the concluding remarks of this work and points to possible future actions.

## 2 UNCERTAINTY QUANTIFICATION AND SENSITIVITY ANALYSIS

The goal of this chapter is to present the concepts and methods for forward uncertainty quantification (UQ) and sensitivity analysis (SA) applied in this work. We begin introducing the idea of uncertainty in the context of mathematical models and proceed by providing an overview of the existing UQ and SA techniques. Essential probability theory concepts are also presented.

### 2.1 MODELS AND UNCERTAINTY

In the field of cardiovascular physiology, as in many other areas of science, experimental techniques are lengthy, costly, hard to reproduce, and, therefore, deficient when there is an interest in understanding complex systems and their underlying dynamics. By combining the physical/physiological laws and experimental data with advanced numerical techniques to solve the equations describing a phenomenon, computer models make up a powerful tool capable of predicting the studied system's events and dynamics.

As a means to improve the simulations of these models, great efforts are made to control the numerical errors of algorithms and to enhance the quality of data acquisition. Despite all this endeavor to reach satisfactory model efficiency levels, predictions of models are always subjected to uncertainty. As pointed out by Saltelli *et al.* (2008, p. 3): “*Uncertainty is not an accident of the scientific method, but its substance*”. In this sense, a model is a tool that can be validated by being capable of repeatedly providing convincing and reliable predictions of the phenomena it represents. Therefore, input uncertainties must be considered ever since the beginning of the modeling process.

When we consider cardiovascular modeling, significant advancement towards model efficiency and data acquisition has been made up to this point. More recently, cardiovascular models are more and more regarded for therapy planning and individualized diagnosis within clinical contexts (3, 8, 9). Given the delicate nature of this application, special efforts must be made to achieve model robustness and accuracy. One of the biggest challenges towards this task is the adjustment of model parameters to patient-specific circumstances. This challenge is directly related to the pervasive and ubiquitous nature of uncertainty within models. Firstly, because clinical data are always hampered with uncertainty and secondly because some model parameters cannot be obtained through data, instead, they are usually obtained through mathematical and physiological considerations, which also introduce uncertainty. In addition to that, one must also consider the inherent biological variability between individual subjects.

Therefore, it is of utmost importance to quantify the uncertainties in the model outputs that originated from uncertainties in the inputs, which is UQ's central role. Another method is SA, which evaluates how sensitive the outputs are to uncertainties at the inputs. It is important to remark that in this work, we limit to perform forward uncertainty quantification of the

models discussed so far. Inverse uncertainty quantification, which aims to estimate the model's parameters and their distribution using experimental data, is not performed.

In the context of cardiovascular modeling, some recent studies analyze and quantify the uncertainties from input data. The use of LP models to simulate phenomena related to the systemic circulation, such as the dynamics of cerebral blood flow with postural changes (30) or the dynamics of the HUT protocol (33), is subjected to uncertainties. The reason is the limited number of measurable input parameters and the inherent biological variability between subjects. Additionally, in clinical contexts, it is not common to perform repeated measurements, which leads to inadequate information about the uncertainty of parameters that can be measured (44), such as the arterial pressure and the cardiac cycle length. These facts are also true for more complex, multi-scale simulations (15, 4, 43), where uncertainties in the ventricular wall thickness, fiber orientation, or the ejection fraction can arise. These uncertainties usually come from measurement variabilities, such as in noisy resonance images, equipment limitations, and user intervention, or variability in mechanical and anatomical parameters.

## 2.2 AN OVERVIEW OF UQ AND SA TECHNIQUES

There are many UQ and SA methods available in the literature. They can be divided into two major groups: the techniques that consider the whole input space in the process of examining the effects of uncertainties on the outputs, which are called global methods; and the methods that, in the other hand, explore the impact of an individual input on the output while keeping all the others fixed, which are called local methods.

Local methods are a derivative-based approach, whose notion of sensitivity is given by the derivative of an output with respect to an input parameter. This way, the inputs' effects on the outputs are examined by looking at the variation around a reference value of one input, while all other inputs are kept fixed. With this approach, it is only possible to obtain information that is local to the input where the derivatives are computed. Therefore, it is impossible to explore the effects on the output caused by the whole input space and their interactions. This means that local methods are misleading when dependencies of the output on the inputs such as non-additivity, non-monotonicity, and non-linearity, exist (3, 34). In the context of cardiovascular modeling for clinical applications, the inputs can be subjected to much uncertainty. The use of global methods is essential and is considered the golden standard for UQ and SA since they explore the space of all the uncertain inputs and make no assumptions about linearity, additivity, or monotonicity (36).

One of the most used global methods is the Monte Carlo (MC) method (35), in which independent realizations (samples) of the inputs are sampled from their prescribed probability density functions. The model is executed with each set of random inputs, and statistical information can be directly calculated from the ensemble of solutions. The MC method is part of the class of non-intrusive global methods, which are methods that do not require changes in

the numerical code of the models. Despite being simple to execute, the MC method can be computationally expensive, as typically, a large number of deterministic simulations are required to obtain a good convergence in the calculation of the solution statistics. The mean value, for example, typically converges with a rate of  $1/\sqrt{K}$ , where  $K$  is the number of samples (35).

Other examples of non-intrusive global methods are: the Lagrangian interpolation method (45), and the generalized polynomial chaos with the probabilistic collocation method (42, 46). The probabilistic collocation method is applied in this work. In intrusive approaches, differently, new governing equations for the model are derived from a parameterization of the uncertainty in the inputs. Examples of intrusive methods are the perturbation method (47), the moment equation method (48), and the gPC with the stochastic Galerkin method (38).

### 2.2.1 Input prioritization and input fixing

To carry out the uncertainty and sensitivity analysis, we regard as an input anything that can introduce variation to the model's output, and the model is, of course, the deterministic tool that can simulate and predict our desired phenomena. The procedure begins with estimating the input parameters, which can be achieved by fitting the output to some observed data. Usually, after determining appropriate parameter values, information about their uncertainty can be characterized in terms of probability density functions of the parameters. This process is known as inverse uncertainty quantification and is not considered in this work. When experimental data is not available for performing an inverse uncertainty quantification, as in the present work, reasonable assumptions about input parameters are assumed for the analyses. After completing the propagation of uncertainties to the model outputs, useful measures can be quantified from the uncertain outputs. Besides, this investigation can be further improved by employing a sensitivity analysis that can assess how influential the input parameters are to the outputs' uncertainty.

It would be desirable to achieve satisfactory simulation accuracy with the least amount of effort possible in a clinical context since it can be expensive and cumbersome to collect proper data from patients. If it is known that some inputs can be measured to their true value, a useful setting for the UQ and SA is the *input prioritization*. In this setting, the true value of the inputs is unknown and the objective is to identify which input, once discovered and fixed at its true value, would reduce the output's uncertainty the most.

Another challenge in the clinical application is to find an adequate level of complexity for the model. Increasing a model's complexity can lead to more accurate predictions. However, at the same time, more inputs must be assessed, which can simultaneously lead to an increase of uncertainty on the output. Therefore, it is essential to consider the amount of uncertainty coming from the model complexity and the amount of uncertainty coming from the data to find an optimal trade-off (31). In general, overly complicated models are infeasible within a clinical scenario because of the high computational effort that is necessary to perform their simulations.

In this case, the balance leans towards a less complicated model, and a useful procedure is the *input fixing*. The objective is to ascertain which of the inputs can be fixed anywhere in their range of variation (e. g. population-based values) without considerably affecting the accuracy of an output of interest. This can be done by analyzing which inputs have a negligible contribution to the output variability given their interactions with other inputs. Analyzing a model in this way could provide insight on how and where to simplify (reduce) a model since entire sections of the model could be lumped together if all parameters involved in that section are noninfluential for simulating a specific scenario.

### 2.3 UNCERTAINTY QUANTIFICATION

To understand the gPC method, used in this work, and how it is applied for the uncertainty quantification, we first introduce the basic notation.

Let the cardiovascular models considered here be represented by a function  $y = f(\mathbf{z})$ , where  $y$  is one deterministic output of interest for the vector of uncertain input parameters  $\mathbf{z} = [z_1, z_2, \dots, z_D]$ , where  $D$  is the number parameters. We assume that the inputs are subject to uncertainties due to measurement errors. As a consequence, the outputs are also affected by these uncertainties. Thus, the functional representation of the model can be written as  $Y = f(\mathbf{Z})$ , where  $Y$  is the stochastic output and  $\mathbf{Z} = [Z_1, Z_2, \dots, Z_D]$  is the stochastic input vector which is a random multivariate variable. The uncertain parameters  $Z_i$  are assumed independent, and its joint probability density function is denoted by  $\rho_{\mathbf{Z}}(\mathbf{z})$ . The output  $Y$  is also a random variable with an associated probability density function  $\rho_Y$ , which depends on  $\mathbf{Z}$  and is governed by the model  $f$ .

To describe the uncertainty in the output  $Y$  the following statistical moments are used: the expected value  $\mu$ , the standard deviation  $\sigma$  and the coefficient of variation  $CoV$ . The expected value (also called the first moment or mean of  $Y$ ) is given by

$$\mu[Y] = \mathbb{E}[Y] = \int_{\Omega_Y} y \rho_Y(y) dy. \quad (2.1)$$

The standard deviation gives the expectation of how much the the output  $Y$  deviates from the mean value, and is given by

$$\sigma[Y] = \sqrt{\mathbb{V}[Y]}, \quad (2.2)$$

where  $\mathbb{V}[Y]$  is the variance or the second moment of  $Y$ , given by

$$\mathbb{V}[Y] = \int_{\Omega_Y} (y - \mathbb{E}[Y])^2 \rho_Y(y) dy. \quad (2.3)$$

Finally, the coefficient of variation is the ratio between the mean and standard deviation, given by

$$CoV[Y] = \frac{\sigma[Y]}{\mu[Y]}. \quad (2.4)$$

Next, the concept of percentiles is introduced. The  $x$ -th percentile of  $Y$  is the value of  $Y$  under which  $x\%$  of observations of  $Y$  are located. For instance, the 10-th percentile of  $Y$ , gives the

value of  $Y$  for which 10% of the model evaluations will give an output lower than the percentile. The  $(\beta \cdot 100)$ -th percentile of  $Y$ , denoted as  $y[\beta]$ , defines a value below which  $\beta \cdot 100$  percent of the observations  $Y$  are located, that is:

$$\beta = \int_{-\infty}^{Y_\beta} \rho_Y(y) dy. \quad (2.5)$$

observations are located. By combining two percentiles, a  $(\beta \cdot 100)\%$  prediction interval (PI) of the outputs

$$I_\beta = [y_{[\beta/2]}, y_{[1-\beta/2]}], \quad (2.6)$$

is defined such that  $I_\beta$  is a range of values such that the probability of finding a value  $y$  outside this range is  $(\beta \cdot 50)\%$  at each side. For instance, 90% prediction interval gives us the interval within which 90% of the  $Y$  outcomes occur, which also means that 5% of the outcomes are above and 5% are below this interval. For this case the PI that covers 90% of the evaluations of  $Y$  is the range  $I_{0.1} = [y_{[0.05]}, y_{[0.95]}]$ .

## 2.4 SENSITIVITY ANALYSIS

Input prioritization and input fixing settings are performed using variance-based metrics known as Sobol' sensitivity indices (49). The first-order or main sensitivity index gives the direct effect of the uncertain input  $Z_i$  on the output by quantifying the portion that  $Z_i$  contributes, without interactions, to the total variance of  $\mathbb{V}[Y]$ . It is given by:

$$S_i = \frac{\mathbb{V}[\mathbb{E}[Y|Z_i]]}{\mathbb{V}[Y]}, \quad (2.7)$$

where  $\mathbb{E}[Y|Z_i]$  represents the expected value of  $Y$  for a fixed value of  $Z_i$ , with  $1 \leq i \leq D$ . The main sensitivity index is useful for input prioritization since it gives the expected reduction in the total variance that could be achieved if the unknown true value of  $Z_i$  could be measured.

The total sensitivity index is the sum of all first and higher-order effects (interactions between inputs) where the uncertain input  $Z_i$  is involved. It is given by

$$S_{T,i} = 1 - \frac{\mathbb{V}[\mathbb{E}[Y|Z_{-i}]]}{\mathbb{V}[Y]}, \quad (2.8)$$

where  $Z_{-i}$  is the set of uncertain inputs except  $Z_i$ . The total sensitivity index represents the variance linked to the effect of all interactions of  $Z_i$  as well as the direct effect of  $Z_i$ . This index is useful for input fixing, since if one input parameter has a negligible value for  $S_{T,i}$ , then it could be fixed within its range of variability.

### 2.4.1 Time series sensitivity analysis

When dealing with non-scalar outputs of interest, such as the left ventricle pressure and volume time series, the sensitivity indices (2.7) and (2.8) are not ideal since they do not account

for the different variance at different points in time. Since the variance is not constant over time, the sensitivity indices at two time instants are locally scaled, and therefore are not comparable.

To compute main and total sensitivity indices for time series, we use the time-averaged and variance-scaled sensitivity indices proposed by (28). For a given uncertain input  $Z_i$ , the time-averaged main sensitivity indices ( $TAS_i$ ) are given by

$$TAS_i = \frac{\int_{t_0}^{t_1} \mathbb{V}[\mathbb{E}[Y|Z_i]]_t dt}{\int_{t_0}^{t_1} \mathbb{V}[Y]_t dt} = \frac{\int_{t_0}^{t_1} S_i(t) \mathbb{V}[Y]_t dt}{\int_{t_0}^{t_1} \mathbb{V}[Y]_t dt}, \quad (2.9)$$

and the time-averaged total sensitivity indices ( $TAS_{T,i}$ ) are given by

$$TAS_{T,i} = \frac{\int_{t_0}^{t_1} (1 - \mathbb{V}[\mathbb{E}[Y|\mathbf{Z}_{-i}]]_t) dt}{\int_{t_0}^{t_1} \mathbb{V}[Y]_t dt} = \frac{\int_{t_0}^{t_1} S_{T,i}(t) \mathbb{V}[Y]_t dt}{\int_{t_0}^{t_1} \mathbb{V}[Y]_t dt}, \quad (2.10)$$

where  $\mathbb{V}[Y]_t$  is the variance of  $Y$  evaluated on time  $t$ .

## 2.5 GENERALIZED POLYNOMIAL CHAOS

For UQ and SA analyses, the gPC method is used to build surrogate models that allow the computation of the metrics described in Sections 2.3 and 2.4. In the gPC method, a model's stochastic response  $Y$ , which is typically a quantity of interest (QoI) derived from the solution of the governing equations, is expanded into a series of orthogonal polynomials, which are functions of the uncertain inputs  $\mathbf{Z}$ .

### 2.5.1 gPC expansion

Given the aforementioned stochastic input vector  $\mathbf{Z} = Z_1, Z_2, \dots, Z_D$ , the stochastic output  $Y$  for a QoI may be expressed by an infinite polynomial chaos expression (42, 50):

$$Y = \sum_{j=0}^{\infty} b_j \Psi_j(\{Z_n\}_{n=1}^{\infty}) = f_{gPC}(\mathbf{Z}), \quad (2.11)$$

where  $b_j$  are the deterministic coefficients to be determined and  $\Psi_j$  are the orthogonal polynomials with respect to the random inputs  $Z_1, Z_2, \dots, Z_n$ .

The mean value of each  $\Psi_j$ , for  $j = 1, \dots, N_p - 1$  is zero for multivariate polynomials constructed from univariate polynomials using the Wiener-Askey scheme (3):

$$\mathbb{E}[\Psi_e] = \int_{\Omega_{\mathbf{Z}}} \Psi_e(\mathbf{z}) \rho_{\mathbf{Z}}(\mathbf{z}) d\mathbf{z} = 0, \quad (2.12)$$

while for  $\Psi_0$  the mean value is 1, since  $\Psi_0 = 1$ . Also, the orthogonality of the multivariate polynomials can be expressed in terms of their inner-product as:

$$\Psi_i \cdot \Psi_j = \int_{\Omega_{\mathbf{Z}}} \Psi_i(\mathbf{z}) \Psi_j(\mathbf{z}) \rho_{\mathbf{Z}}(\mathbf{z}) d\mathbf{z} = \delta_{ij} H_i, \quad (2.13)$$

where  $\delta_{ij}$  is the Kronecker delta and  $H_i$  is a normalization factor associated to  $\Psi_i$ .

In practice, the expansion (2.11) is usually truncated by finite terms and the approximation of  $Y$ , known as the surrogate model  $\hat{Y}$  can be expressed as:

$$f(\mathbf{Z}) = Y \approx \hat{Y} = \sum_{j=0}^{N_p-1} c_j \Psi_j(\mathbf{Z}) = f_{gPC}(\mathbf{Z}), \quad (2.14)$$

where  $c_j$  are the expansion coefficients to be determined and  $\Psi_j(\mathbf{Z})$  are orthogonal polynomials. The polynomial expansion (2.14) of degree  $p$  for  $D$  stochastic inputs has  $N_p$  terms, which is computed as

$$N_p = \frac{(D+p)!}{D!p!}. \quad (2.15)$$

The original polynomial chaos scheme (37) used Hermite polynomials as the basis functions  $\Phi_j(\mathbf{Z})$  and Gaussian random variables. Considering  $\rho_z(z)$  as a weight function in the inner-product of equation (2.13), the original scheme was further generalized (38) to handle other random variables, which established a correspondence between the distribution of the random variable and the type of orthogonal polynomials used as the basis functions (3, 35).

### 2.5.2 Determination of the expansion coefficients

By estimating the coefficients  $c_j$  for the general expression in Equation (2.14) the expansion can be specified for each QoI. The most common non-intrusive approaches for the determination of the coefficients are the pseudo-spectral projection and the point collocation method (51). The point collocation method is applied in this work.

In the point collocation method (or probabilistic collocation method) (46) we start by defining a stochastic residual dependent on the random inputs  $\mathbf{Z}$  and the coefficients  $c_j$ :

$$R(\{c_j\}, \mathbf{Z}) = \hat{Y} - Y, \quad (2.16)$$

where  $Y$  is the model output and  $\hat{Y}$  is the surrogate model output. The set of coefficients  $c_j$  are obtained through a weighted residual formulation in the random space, given by

$$\int_{\mathbf{Z}} R(\{c_j\}, \mathbf{Z}) w_i(\mathbf{Z}) \rho_{\mathbf{Z}} d\mathbf{Z} = 0, \quad i = 0, 1, \dots, N_p - 1, \quad (2.17)$$

where  $w_i(\mathbf{Z})$  are the weighting functions and  $\rho_{\mathbf{Z}}$  is the joint probability density function of the stochastic input vector  $\mathbf{Z}$ . When the weighting functions chosen are the same as the basis functions used in the series expansion (2.14), exponential convergence with respect to the polynomial order of the weighting functions is achieved. This is a common approach known as the Galerkin method, which is an intrusive method and therefore, harder to implement, since it requires modifications on the deterministic solver (42).

In the probabilistic collocation method the weighting functions are defined as

$$w_i(\mathbf{Z}) = \delta(\mathbf{Z} - \mathbf{Z}_i), \quad i = 0, 1, \dots, N_p - 1. \quad (2.18)$$

Here  $\mathbf{Z}_i$  are a particular set of collocation points and  $\delta$  is the Dirac delta function. By applying (2.18) in the weighted residual expression (2.17) and regarding the properties of the Dirac delta function, the following set of equations is obtained:

$$R(\{c_j\}, \mathbf{Z}_i) = 0, \quad i = 0, 1, \dots, N_p - 1, \quad (2.19)$$

which from (2.16) becomes equivalent to

$$f_{gPC}(\mathbf{Z}_i) = f(\mathbf{Z}_i), \quad i = 0, 1, \dots, N_p - 1. \quad (2.20)$$

Introducing the expression of the surrogate model (2.14), the relation (2.20) becomes a system of linear equations  $\mathbf{M}\mathbf{c} = \mathbf{y}$ , given by:

$$\underbrace{\begin{bmatrix} \Psi_0(\mathbf{Z}_{(1)}) & \Psi_1(\mathbf{Z}_{(1)}) & \dots & \Psi_{N_p-1}(\mathbf{Z}_{(1)}) \\ \Psi_0(\mathbf{Z}_{(2)}) & \Psi_1(\mathbf{Z}_{(2)}) & \dots & \Psi_{N_p-1}(\mathbf{Z}_{(2)}) \\ \vdots & \vdots & \ddots & \vdots \\ \Psi_0(\mathbf{Z}_{(N_p-1)}) & \Psi_1(\mathbf{Z}_{(N_p-1)}) & \dots & \Psi_{N_p-1}(\mathbf{Z}_{(N_p-1)}) \end{bmatrix}}_{\mathbf{M}} \underbrace{\begin{bmatrix} c_0 \\ c_1 \\ \vdots \\ c_{N_p-1} \end{bmatrix}}_{\mathbf{c}} = \underbrace{\begin{bmatrix} f(\mathbf{Z}_{(1)}) \\ f(\mathbf{Z}_{(2)}) \\ \vdots \\ f(\mathbf{Z}_{(N_p-1)}) \end{bmatrix}}_{\mathbf{y}}. \quad (2.21)$$

Here  $N_s \geq N_p$  is the number of collocation points. It is recommended that the number of samples used should be greater than  $N_p$ , which leads to an overdetermined system that is solved using linear least squares methods in the ChaosPy library (3, 51).

### 2.5.3 UQ and SA metrics from the gPC

Once the expansion coefficients are computed from the system (2.21), the surrogate model  $f_{gPC}(\mathbf{Z})$  can be used to calculate the UQ and SA metrics given in Sections 2.3 and 2.4. The orthogonal nature of the expansion functions used guarantees an easy expression for obtaining the expected value and the variance (3). By applying the surrogate model on the Equations (2.1) and (2.3), the expected value  $\mu[Y]$  and variance  $\mathbb{V}[Y]$  can be simply obtained. First, we show that the expected value can be simply evaluated as the first expansion coefficient, that is:

$$\begin{aligned} \mathbb{E}[Y] &\approx \mathbb{E}[\hat{Y}] = \mathbb{E}[f_{gPC}(\mathbf{Z})] = \mathbb{E}\left[\sum_{j=0}^{N_p-1} c_j \Psi_j(\mathbf{Z})\right] \\ &= \int_{\Omega_{\mathbf{Z}}} \sum_{j=0}^{N_p-1} c_j \Psi_j(\mathbf{Z}) \rho_{\mathbf{Z}}(\mathbf{z}) d\mathbf{z} = \sum_{j=0}^{N_p-1} c_j \int_{\Omega_{\mathbf{Z}}} \Psi_j(\mathbf{Z}) \rho_{\mathbf{Z}}(\mathbf{z}) d\mathbf{z} \\ &= \sum_{j=0}^{N_p-1} c_j \mathbb{E}[\Psi_j] = c_0 \mathbb{E}[\Psi_0] + c_1 \mathbb{E}[\Psi_1] + \dots + c_{N_p-1} \mathbb{E}[\Psi_{N_p-1}] \\ &= c_0, \end{aligned} \quad (2.22)$$

where the zero-mean property (2.12) of the polynomials and the fact that  $\mathbb{E}[\Psi_0] = 1$  have been used. Following a similar procedure as performed for the expected value, the variance can be

computed as

$$\mathbb{V}[Y] = \sum_{j=1}^{N_p-1} c_j^2 \mathbb{E}[\Psi_j^2(\mathbf{Z})]. \quad (2.23)$$

The standard deviation  $\sigma[Y]$  and the coefficient of variation  $CoV[Y]$  are easily obtained from (2.22) and (2.23). The computation of Sobol' indices is performed by exploiting the properties of the polynomials in the expansion, as in the method described in (50). The percentiles cannot be directly computed from the gPC expansion. However, it is possible to apply the Monte Carlo method with the surrogate model  $f_{gPC}(\mathbf{Z})$  to estimate the percentiles instead of using the forward model  $f(\mathbf{Z})$ .

## 2.6 ACCURACY OF THE SURROGATE MODEL

The accuracy of the surrogate model produced by the gPC method depends on the polynomial degree  $p$  and the number of samples  $N_s$ . As previously mentioned, normally choosing the number of samples as  $N_s = mN_p$ , where  $m > 1$  yields better accuracy (3), and requires the solution of a least squares problem. To check the accuracy of the surrogate model  $Y \approx f_{gPC}(\mathbf{Z})$  we used the leave one out cross validation (LOO) approach (52).

The LOO cross validation approach takes one sample out of the  $N_s$  samples available and then builds the surrogate model with  $N_s - 1$  samples. This is performed for  $i = 1, \dots, N_s$  times, leaving at each time one different sample out of the construction of the polynomial. Let  $\hat{Y}_i$  be the model output computed by the  $i$ -th gPC approximation, whereas  $Y_i$  is the forward model output for the  $i$ -th sample left out. Thus, the predicted residual is given by

$$\Delta_i = Y_i - \hat{Y}_i, \quad (2.24)$$

and the approximation error is the mean value of the squared predicted values

$$Err_{LOO} = \frac{1}{N_s} \sum_{i=1}^{N_s} (\Delta_i)^2. \quad (2.25)$$

We calculate the determination coefficient to evaluate the accuracy of the gPC approximations and assess its convergence using the following metric (52):

$$Q^2[f_{gPC}(\mathbf{Z})] = 1 - \frac{Err_{LOO}}{\mathbb{V}[Y]}. \quad (2.26)$$

The closer the value of  $Q^2$  is to 1, the more accurate is the surrogate model.

In general, with a larger the number of samples and the moderate polynomial degree, the better is the accuracy of the surrogate model. However, increasing both results in a excessive number of evaluations of the forward model (lumped parameter model or coupled model), which might be prohibitive, specially for the coupled model which requires the solution of a nonlinear partial differential equation.

Thus, in order to achieve a reasonable accuracy for the surrogate model, we started creating a low polynomial degree and using a small number of samples, until we found a combination of  $p$  and  $N_s$  that yields a good accuracy for the gPC in terms of the LOO cross validation.

## 2.7 THE ChaosPy TOOLBOX

Implementing the whole UQ and SA procedure from scratch can certainly be quite burdensome and should not be considered, as there are several ready-made tools to be used. The ChaosPy toolbox (51) implemented in Python is one of them, and the one used in this work. It is designed to be modular, flexible and easy to use, by combining a lot of fundamental and advanced building blocks. It offers a wide set of pre-defined competitive statistical methods and is aimed for analysing uncertainty using Monte Carlo simulations or polynomial chaos expansions.

With the ChaosPy toolbox one can generate random variables, construct polynomials, make use of sampling schemes, numerical integration rules, and point collocation. Additionally, it is possible to add user defined functionality to all the aforementioned features. Next, we consider a simple theoretical example to show the capabilities of this toolbox for performing uncertainty and sensitivity analysis.

### 2.7.1 An illustrative example

Consider the simple equation for the logistic growth model, given by

$$\frac{dP}{dt} = rP \left( 1 - \frac{P}{K} \right), \quad (2.27)$$

where  $P$  represents the size of a given population,  $t$  is the time in years,  $r$  is the growth rate and  $K$  is the population's carrying capacity. This ordinary differential equation can easily be solved in Python using, for example, the explicit Euler method:

Listing 2.1 – Python code for solving the logistic growth model.

---

```

1 def model(P_0, r, K, t):
2     P = np.empty(len(t))
3     P[0] = P_0 # initial condition
4     for n in xrange(len(t) - 1):
5         dt = t[n+1] - t[n]
6         P[n+1] = P[n] + dt*r*P[n]*(1.0 - P[n]/K)
7
8     # find the inflection point
9     dP = np.gradient(P)

```

```

10     dP2 = np.gradient(dP)
11     inflect = np.argmax(dP2 < 0)
12
13     return P, t[inflect]

```

---

In the code above, the model returns the solution curve and the year of the inflection point, which is the year when the population stops to grow exponentially. This definition of the model can be regarded as the forward model  $f(\mathbf{Z})$ , where the stochastic input vector  $\mathbf{Z}$  is comprised of the uncertain inputs for the growth rate  $r$ , and the carrying capacity  $K$ . Suppose that  $r$  follows a Gaussian distribution and  $K$  has an uniform distribution, and assume that they are independent, then their joint probability density function can be obtained with ChaosPy as:

Listing 2.2 – Python code for defining the joint distribution of the random inputs.

```

1 import chaospy as cp
2
3 # growth rate
4 Z0 = cp.Normal(1.0, 2.0)
5 # carrying capacity
6 Z1 = cp.Uniform(150000, 250000)
7 distribution = cp.J(Z0, Z1)

```

---

The arguments for the `cp.Uniform` method are the lower and upper thresholds of the distribution, respectively, while for the `cp.Normal` the arguments are the mean and standard deviation of the distribution, respectively. Now, if one needs to take 200 samples, and then evaluate the forward model, the code is as simple as:

Listing 2.3 – Python code for sampling points and evaluating the forward model.

```

1 samples = distribution.sample(200)
2 evals = [model(200, Z[0], Z[1], t)[0] for Z in samples.T]

```

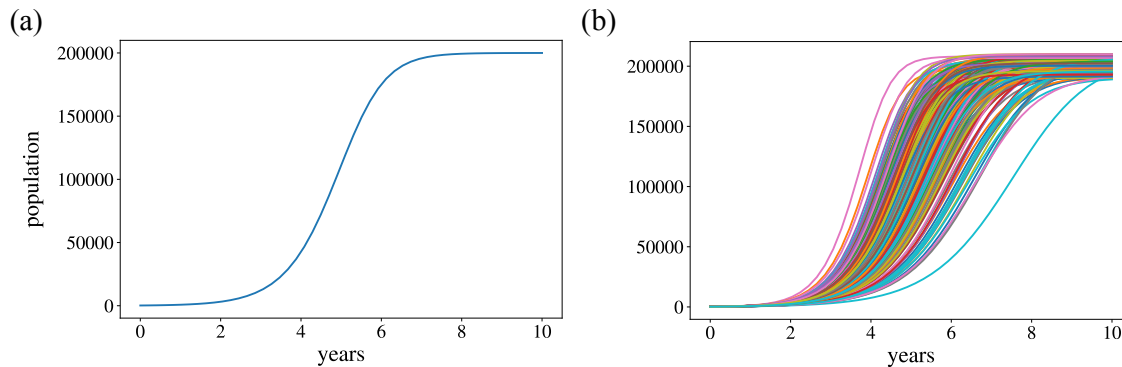
---

The left panel of Figure 1 shows the solution of the deterministic model for a population starting with 200 individuals, and a growth rate of  $r = 1.6$  and a carrying capacity of  $K = 200000$ . The right panel shows the 200 evaluations of the stochastic model.

## 2.7.2 Example of UQ and SA

The sampling procedure just described is the way to perform the Monte Carlo method using the the ChaosPy toolbox. The forward model can be evaluated for any QoI and the desired

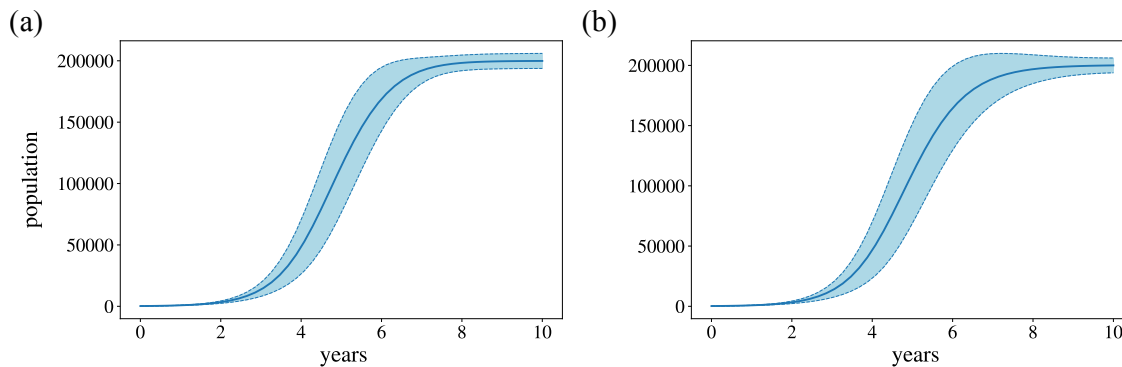
Figure 1 – The logistic growth model; (a) Deterministic solution; (b) Evaluations of the stochastic forward model.



Source: Elaborated by the author.

UQ and SA metrics for the particular QoI can be calculated. One QoI could be the logistic curve itself, so one could take the evaluations of the forward model and compute its expected value and standard deviation, as shown in Figure 2.

Figure 2 – Monte Carlo simulation of the logistic growth model; (a) Expected value  $\pm$  standard deviation for 50 evaluations; (b) Expected value  $\pm$  standard deviation for 200 evaluations.



Source: Elaborated by the author.

Suppose now we want to analyse the effects of uncertainties in the growth rate and the carrying capacity when evaluating the year when the inflection point occurs. To compute the desired metrics for this QoI using the gPC approach, one should first obtain the joint probability density function of the uncertain inputs, just as we did in Listing 2.2. Next, the stochastic input points should be sampled as in the Monte Carlo simulation, choosing a number of samples equal to or greater than the number of terms, given by Equation (2.15). With the uncertain inputs sampled, the forward model can be evaluated for the desired QoI, and the surrogate model can be obtained by fitting the polynomial to the samples using the probabilistic collocation method,

as shown in Listing 2.4.

Listing 2.4 – Python code for creating the gPC expansion.

---

```

1 p = 3 # polynomial degree
2 Np = factorial(2 + p) / (factorial(2) * factorial(p))
3 m = 3 # multiplicative factor
4 Ns = m * Np # number of samples
5 samples = distribution.sample(Ns)
6 evals = [model(200,Z[0],Z[1],t)[1] for Z in samples.T]
7 poly_exp = cp.orth_ttr(p,distribution)
8 surr_model = cp.fit_regression(poly_exp,samples,evals)

```

---

We create a polynomial expansion of degree  $p = 3$  using an orthogonal basis with the method `cp.orth_ttr`, then, with the samples, evaluations and polynomial expansion available, the surrogate model is created using the method `cp.fit_regression`.

With the surrogate model available, analysis can be done by computing the UQ and SA metrics desired:

Listing 2.5 – Python code for obtaining the UQ and SA metrics.

---

```

1 mean = cp.E(surr_model, distribution)
2 std = cp.Std(surr_model, distribution)
3 sm = cp.Sens_m(surr_model, distribution)
4 st = cp.Sens_t(surr_model, distribution)

```

---

The expected value  $\mu[Y]$  and standard deviations  $\sigma[Y]$  are obtained with the methods `cp.E` and `cp.Std`, respectively, while the Sobol's main  $S_i$  and total  $S_{T,i}$  sensitivity indexes for the parameters  $r$  and  $K$  ( $i = r, K$ ) are obtained with the methods `cp.Sens_m` and `cp.Sens_t`, respectively. The year of the inflection point in the logistic growth curve was considered as a QoI. Table 1 shows the results of the analysis for this QoI. It is possible to note that the growth rate is the most influential input when measuring this QoI.

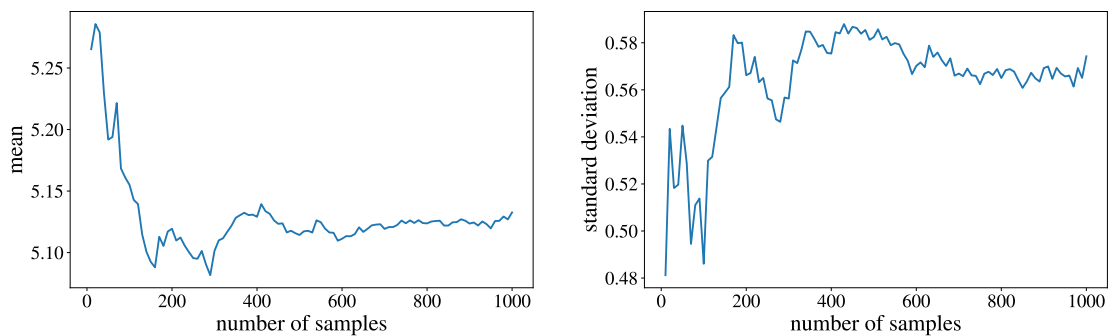
Table 1 also shows the effects of choosing different combinations of the polynomial degree  $p$  and the multiplicative factor  $m$ . One can see that, as the polynomial degree increases, the mean and standard deviation converge to a specific value. This confirms that the gPC method can be accurate enough (in terms of the determination coefficient  $Q^2$ ) with a small number of samples  $N_s$ . Figure 3 shows the computed mean values and standard deviations for the inflection point using the Monte Carlo method. It is evident that it requires a larger number of samples to converge to values similar to those obtained with the gPC method.

Table 1 – UQ and SA results for the logistic growth model:  $p$  is the polynomial degree,  $m$  the multiplicative factor of the minimum number of samples required  $N_s$  the number of samples used to create the surrogate model, and  $Q^2$  is the determination coefficient.

$p$	$m$	$N_s$	$\mu[Y]$	$\sigma[Y]$	$S_r$	$S_K$	$S_{T,r}$	$S_{T,K}$	$Q^2$
1	1	3	6.404	2.816	0.772	0.228	0.772	0.228	0.781
1	2	6	5.069	0.485	0.985	0.015	0.985	0.015	0.902
2	1	6	4.951	0.582	0.683	0.244	0.765	0.317	0.343
2	2	12	5.126	0.566	0.996	0.003	0.996	0.003	0.857
2	3	18	5.130	0.560	0.988	0.012	0.988	0.012	0.914
3	2	20	5.125	0.557	0.992	0.006	0.994	0.008	0.902
3	3	30	5.135	0.529	0.985	0.001	0.999	0.015	0.908

Source: Elaborated by the author.

Figure 3 – Mean value and standard deviation convergence for the Monte Carlo method.



Source: Elaborated by the author.

### 3 CARDIOVASCULAR MODELS

The function of the left ventricle and systemic arteries within the cardiovascular system provides important hemodynamic parameters for clinical assessment. By measuring quantities such as ventricular and arterial blood volumes and pressures at crucial moments of a cardiac cycle, one can trace the overall situation of a given patient and, through these measures, obtain insights and design proper treatments and therapies (53).

This chapter considers two closed-loop pulsatile LP models, one having five compartments and other with three-compartments. We also discuss one coupled model of the systemic circulation composed by the three-compartment LP model and an electromechanical model of the left ventricle simulated by three-dimensional FE method.

The underlying physiological notions for understanding the models are presented in the first section of this chapter. In the following sections, all the mathematical equations, numerical techniques used in the models for numerical simulations are described.

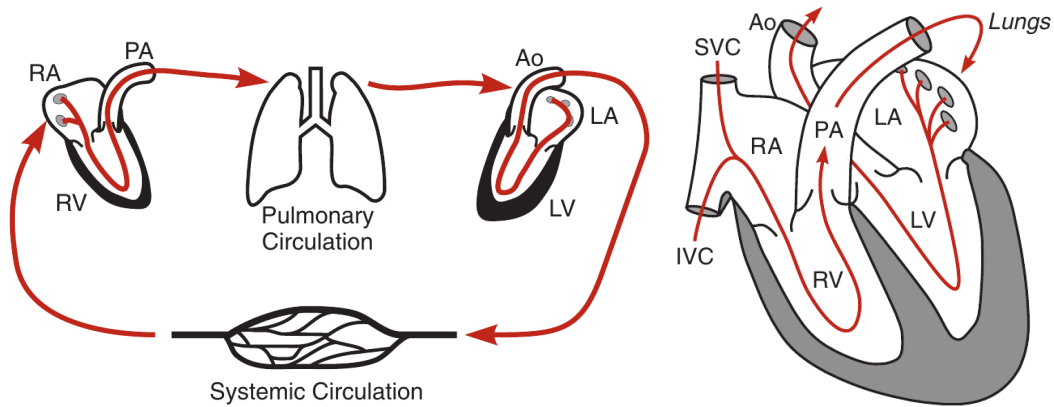
#### 3.1 CARDIOVASCULAR PHYSIOLOGY BACKGROUND

For cells to function correctly, they need mechanisms that allow them to acquire metabolic substrates from the external environment and remove byproducts of metabolism. In large organisms, these exchanges are made possible by a complex blood vessel system that exchanges substances between cells and blood and between blood and environment. This complex system of blood vessels is the cardiovascular system (Figure 4), which is made of the systemic circulation, the pulmonary circulation, and the heart connecting these two parts closing a circulatory loop (54, 55, 56, 57, 58).

The heart can be seen as a pair of pumps that ensure correct blood flow throughout the muscles and organs. The heart's left side consists of the left ventricle and the left atrium, while the right side of the heart consists of the right ventricle and the right atrium. The right side is anatomically smaller than the left side of the heart. The left ventricle pumps blood into the systemic circulation through the aorta. This way, oxygen-rich blood flows through a branch of progressively smaller vessels, from the aorta to the small arteries, then to the arterioles, until it reaches the capillaries, where the exchange of oxygen and carbon dioxide occurs.

Blood leaves the systemic capillaries carrying less oxygen and more carbon dioxide and enters the systemic veins and flows through a vasculature that branches into progressively larger vessels until it reaches the right atrium. Blood is discharged from the capillaries into the venules; then, it flows through the small veins entering the vena cava, which transports it to the right atrium. Next, blood goes from the right atrium to the right ventricle, which pumps it into the pulmonary circulation. The partly de-oxygenated blood flows into the lung tissues through the pulmonary capillaries from the pulmonary arteries, where carbon dioxide is exchanged

Figure 4 – Schematic diagram of the cardiovascular system circulation. On the left is an overview of the cardiovascular circuit. On the right is an overview of the blood flow within the heart. RA, right atrium; RV, right ventricle; PA, pulmonary artery; Ao, aorta; LA, left atrium; LV, left ventricle; SVC, superior vena cava; IVC, inferior vena cava.



Source: Adapted from Klabunde (2011).

for oxygen. Finally, the (re-)oxygenated blood leaves the pulmonary capillaries, going to the pulmonary veins and flowing back to the heart's left side, thus completing the circulation. This whole circuit can take about a minute to occur.

There is a structural symmetry between the systemic and pulmonary circulations. When translating their dynamics into mathematical equations, it is expected that systemic and pulmonary circulations equations look the same. The same happens to the heart's left and right sides and their relationship with the systemic and pulmonary circulations. However, despite the similarities in the equations' forms due to symmetry, there are significant quantitative differences in pressure and blood volume. Systemic arterial pressure is about six times greater than the pulmonary arterial pressure. The pulmonary circulation has about 14% of the total blood volume, while the systemic circulation has approximately 74%, whereas the heart has the remaining 12% of the total volume (Table 2).

Table 2 – Normal resting pressure ( $P$ ) and volume ( $V$ ) of the systemic and pulmonary vessels.

	$P$ (mmHg)	$V$ (litres)
systemic arteries	100	1.0
systemic veins	2	3.5
pulmonary arteries	15	0.1
pulmonary veins	5	0.4

Source: Adapted from Hoppensteadt and Peskin (2012).

Also, since the left side of the heart, the systemic circulation, the right side of the heart, and the pulmonary circulation have an in-series relationship, the output of each side of the heart must be balanced. More details on cardiovascular circulation can be found in (54, 57).

### 3.1.1 The cardiac cycle

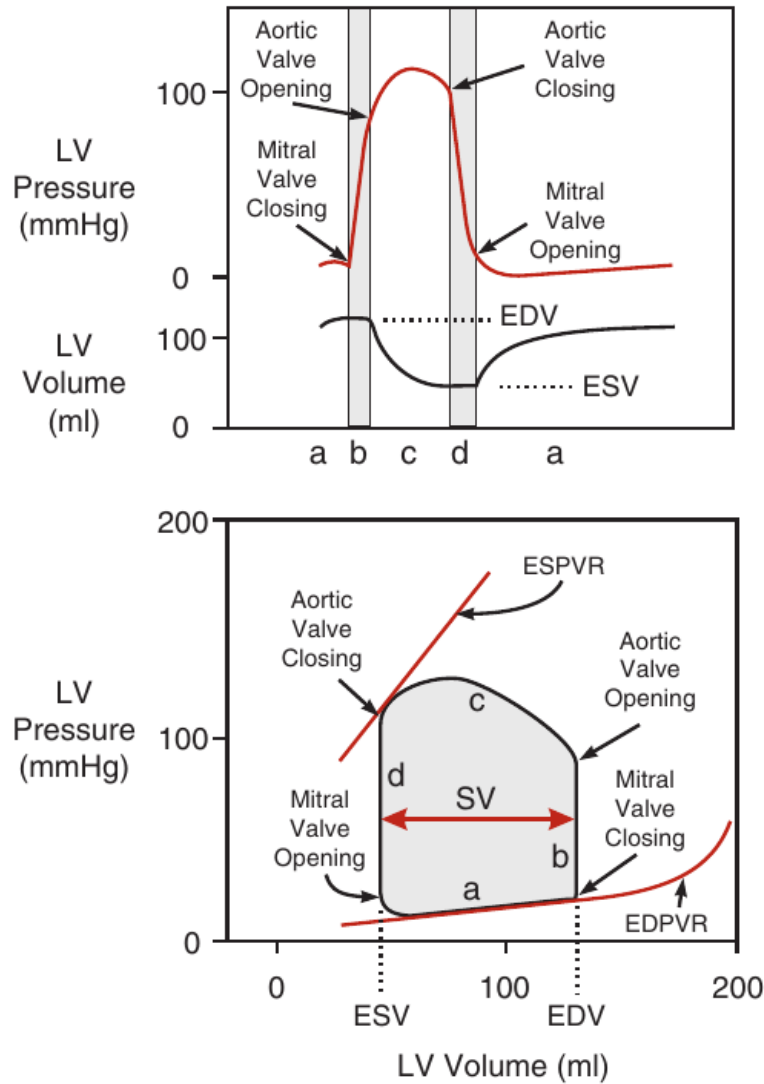
The heart's pumping activity is regulated by the four chambers and four valves between the atria and the ventricles, and between the ventricles and the outflow arteries. The tricuspid valve is located between the right ventricle and the right atrium. Between the left ventricle and the left atrium is located the mitral valve. The pulmonary valve is located at the outflow from the right ventricle. At the outflow from the left ventricle is located the aortic valve.

The cardiac cycle is the name given to the events from the beginning of one heartbeat to the beginning of the next pulse. It consists of a period of relaxation when the heart fills with blood, and a period of contraction, during which the heart ejects the blood into the arterial blood vessels. The relaxation period is called diastole, and the contraction period is called systole.

In Figure 5, the top panel shows the variation of left ventricular pressure (LV pressure) and volume (LV volume) during the time during a complete cardiac cycle. When we consider the left ventricular function during a cardiac cycle, an important diagram is the pressure-volume loop obtained by plotting the left ventricular pressure against the left ventricular volume during the full cycle. Therefore, the pressure-volume loop is a representation of the phase plane, where the time is implicit. As shown in the bottom panel of Figure 5, the pressure-volume loop is made up of four phases, labeled from **(a)** to **(d)**.

The systole begins with the contraction of the left ventricle muscles due to electrical stimulation, which is the phase **(b)** in Figure 5. At this point, all valves are closed, and an isovolumetric increase of ventricular pressure occurs. When it is the same as the arterial pressure, which is about  $80 \text{ mmHg}$ , the aortic valve opens, starting phase **(c)**, and blood is ejected into the aorta, while the pressure rises and then falls according to muscle contraction. The maximum ventricular pressure is achieved at this phase and is about  $120 \text{ mmHg}$ . At the end of this phase, when ventricular pressure drops below the arterial pressure, the aortic valve closes and concludes systole phase. During this phase, ventricular volume decreases while blood is ejected into the aorta and the end of ejection leaves a residual blood in the ventricle, which is called the end-systolic volume (ESV), and is about  $50 \text{ ml}$ . With the closure of the aortic valve, a period of isovolumetric relaxation begins (phase **(d)**), corresponding to the onset of diastole. At this phase all valves are closed and ventricular pressure drops until it is below atrial pressure. At this point the mitral valve opens and phase **(a)** begins. In this phase, left ventricle starts to fill with venous blood flowing from the atrium. Since the muscles are still relaxing, pressure continues to drop until it reaches the minimum ventricular pressure at about  $8 \text{ mmHg}$ . Once the ventricle is at maximal relaxation, the pressure begins to rise again as it fills. At the end of diastole the ventricle is fully loaded and the cardiac cycle ends. The maximum amount of blood inside the filled ventricle is called the end-diastolic volume (EDV), which is about  $120 \text{ ml}$ . The difference between EDV and ESV is called stroke volume (SV) and is about  $70 \text{ ml}$ . The ratio between the SV and the EDV represents the ejection fraction (EF) of the ventricle and is typically greater than.

Figure 5 – Top: Left ventricular pressure and volume during a full cardiac cycle; EDPVR: end-diastolic pressure-volume relationship; ESPVR: end-systolic pressure-volume relationship; a: ventricular filling; b: isovolumetric contraction; c: ventricular ejection; d: isovolumetric relaxation.



Source: Klabunde (2011).

The red curves in the bottom panel of Figure 5 are the end-diastolic pressure-volume relationship (EDPVR) and the end-systolic pressure-volume relationship (ESPVR). The filling phase moves along the EDPVR, also called the passive filling curve of the ventricle. The ESPVR describes the maximal ventricular pressure that can be reached at any given ventricular volume, meaning that the pressure-volume loop cannot cross over it 0.55 (54). Table 3 shows normalized values for some of the aforementioned left ventricular hemodynamic parameters, with differentiation into males and females by age deciles.

Table 3 – Normal left ventricular hemodynamic values by age deciles for male and female subjects; Max AP: maximum arterial pressure; Min AP: minimum arterial pressure; CI: confidence interval; SD: standard deviation.

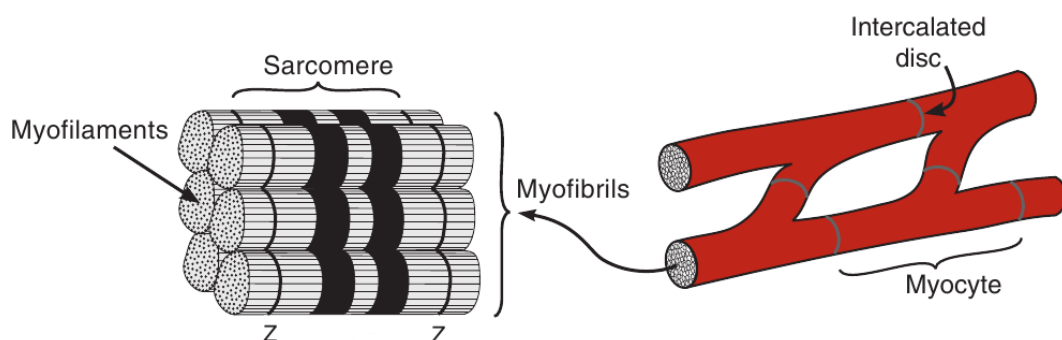
Hemodynamic Value	20 - 29 years	30 - 39 years	40 - 49 years	50 - 59 years	60 - 69 years
			<b>male</b>		
EDV [ml] (mean, 95% CI)	167 (126 , 208)	163 (121, 204)	159 (117, 200)	154 (113, 196)	150 (109, 191)
ESV [ml] (mean, 95% CI)	58 (35, 80)	56 (33, 78)	54 (31, 76)	51 (29, 74)	49 (27, 72)
SV [ml] (mean, 95% CI)	109 (81, 137)	107 (79, 135)	105 (77, 133)	103 (75, 131)	101 (73, 129)
EF [%] (mean, 95% CI)	65 (57, 74)	66 (57, 75)	66 (58, 75)	67 (58, 76)	67 (58, 76)
Max AP [mmHg] (mean, $\pm$ SD)	125 $\pm$ 7	130 $\pm$ 4	123 $\pm$ 3	123 $\pm$ 9	126 $\pm$ 7
Min AP [mmHg] (mean, $\pm$ SD)	73 $\pm$ 5	77 $\pm$ 5	73 $\pm$ 4	77 $\pm$ 6	75 $\pm$ 7
			<b>female</b>		
EDV [ml] (mean, 95% CI)	139 (99, 179)	135 (94, 175)	130 (90, 171)	126 (86, 166)	122 (82, 162)
ESV [ml] (mean, 95% CI)	48 (29, 66)	45 (27, 64)	43 (25, 62)	41 (22, 59)	39 (20, 57)
SV [ml] (mean, 95% CI)	91 (63, 119)	89 (61, 117)	87 (59, 115)	85 (57, 113)	83 (56, 111)
EF [%] (mean, 95% CI)	66 (56, 75)	66 (57, 75)	67 (58, 76)	68 (59, 77)	69 (60, 78)
Max AP [mmHg] (mean, $\pm$ SD)	121 $\pm$ 12	123 $\pm$ 6	115 $\pm$ 13	116 $\pm$ 18	119 $\pm$ 14
Min AP [mmHg] (mean, $\pm$ SD)	70 $\pm$ 9	68 $\pm$ 4	71 $\pm$ 9	71 $\pm$ 11	73 $\pm$ 6

Source: Adapted from Maceira *et al.* (2006).

### 3.1.2 Heart contraction

The pumping action of the heart is made possible by the contraction of its muscle fibers, which receive energy from biochemical processes and develops a force that manifests as an increasing cavity pressure (58). The cardiac muscle is made up of cells called cardiac myocytes (see Figure 6), which arrange themselves as a branching network of cells that allow cell-to-cell conduction of electrical signals thanks to the low-resistance pathways between the cells. This configuration of the cardiac cells permits the heart to contract synchronously.

Figure 6 – Cardiac myocyte structure. Myocytes are joined together by intercalated discs and are composed of myofibrils, which in turn are composed of thick and thin filaments. Between the Z-lines lies the sarcomere.



Source: Adapted from Klabunde (2011).

As shown in Figure 6, the cardiac myocytes are composed of myofibrils that are bundled together in a parallel fashion. The myofibrils are in turn, made up of parallel bundles of thick and thin myofilaments lying between the Z-lines. The segment between the Z-lines is called the sarcomere, which is the basic contractile unit of a myocyte. The length of the sarcomere plays an

important role in the determination of the force of myocyte contraction (57). During the process called excitation-contraction coupling, an active force is developed as the distance between neighboring Z-lines shortens and the overlap between the myofilaments increases. Chemical interactions between the thick and thin filaments cause a shortening of the sarcomere as the filaments slide past each other. The protein interactions involved in the sarcomere shortening are responsible for the active force that makes the myocyte contract.

Preload and afterload are two important physiological concepts related to cardiac muscle contraction. The preload is the initial stretching of the cardiac myocyte as the muscle begins to contract, and is usually associated to the pressure at the end of diastole, that is, the pressure when the ventricle has become filled. The afterload is the load against which the muscle exerts its contractile force, which is considered to be the aortic pressure that the ventricle must overcome to eject blood, commonly referred to as the systolic pressure (54, 57).

### 3.2 LUMPED PARAMETER CIRCULATORY MODELS

Cardiovascular LP models provide an adequate description of the global hemodynamics in the entire circulation by employing only the global variables and parameters of the system in modeling. LP models are also called zero-dimensional, or 0D, models since, at any instant in time, they assume a uniform distribution of the fundamental variables within any compartment (organ or vessel). Though simple, this type of representation can yield accurate quantitative predictions of the cardiovascular system function (18).

The fundamental variables when modeling the cardiovascular dynamics are pressure, flow, and volume. There is a close correlation between the blood flow in the circulatory loop and the electric conduction in a circuit. Blood flow-rate and pressure and their interactions are analogous to current and voltage and their interactions. The resistance and capacitance properties in an electric circuit can be seen as the properties of resisting blood friction and elasticity of a vessel, for example. Therefore, cardiovascular dynamics are often studied and represented in an analogous way to the well-established methods for analyzing electric circuits. However, when dealing with cardiovascular dynamics, special attention must be paid to nonlinearities, like the pressure-volume relationship in a real vessel, as the electrical analogue is unable to express such nonlinearities (18).

The blood can be considered as an incompressible fluid; therefore the amount of blood in any part of the circulation can be directly measured as the volume of blood, in *millilitres (ml)* and denoted by  $V$ . The blood pressure  $p$  within a particular compartment is given by the difference from a reference pressure and is measured in *millimetres of mercury (mmHg)*. The atmospheric pressure is the pressure outside most of the blood vessels, so it is commonly considered as the reference pressure. The blood flow, given by *millilitres by seconds (ml/s)* and represented by  $q$ , is measured as the volume of blood passing a particular point of the circulation per unit of time.

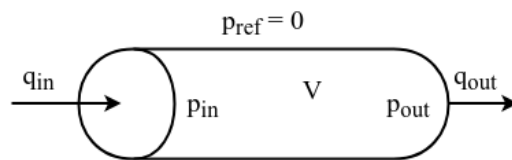
The blood that is pumped from either side of the heart is called the cardiac output (CO) and is the most important measure of flow in the circulation (55). It can be measured as the product of the SV and the number of heartbeats per unit of time, which is the heart rate. Thus, if a person has an SV of  $70 \text{ ml/beat}$  and a heart rate of  $1.3 \text{ beats/s}$ , her cardiac output will be of  $91 \text{ ml/s}$ .

Two important properties of a blood vessel are resistance and compliance. Although any vascular district has these properties, some are more rigid, while others are more complacent. The resistance of a blood vessel is the ability that it has of opposing the blood flow. A rigid vessel has negligible deformation when subjected to an increase in pressure. Figure 7 shows a rigid vessel with resistance  $R$  subjected to an inflow  $q_{in}$  at pressure  $p_{in}$ , and an outflow  $q_{out}$  at pressure  $p_{out}$ . The external pressure is the reference, or atmospheric, pressure  $p_{ref} = 0$ . Since the vessel is rigid, its volume  $V$  is known and constant. Considering the vessel is in a steady-state, then the outflow and inflow are equal, that is  $q_{in} = q_{out} = q$ . A relationship between the pressures  $p_{in}$ ,  $p_{out}$  and the flow  $q$  can be defined as

$$q = \frac{p_{in} - p_{out}}{R}. \quad (3.1)$$

A vessel that satisfies Equation (3.1) is called a resistance vessel and the resistance  $R$  is measured in  $\text{mmHg s/ml}$ .

Figure 7 – A resistance vessel;  $p_{ref}$ : reference pressure;  $q_{in}$ : inflow;  $q_{out}$ : outflow;  $p_{in}$ : upstream pressure;  $p_{out}$ : downstream pressure;  $V$ : constant volume.



Source: Elaborated by the author.

Differently, a complacent vessel, or compliance vessel, has no resistance to blood flow, thus the pressures at its both ends are equal ( $p_{in} = p_{out} = p$ ) for any given flow  $q$ . As shown in Figure 8, when a nonzero pressure variation is applied to a compliance vessel, a volume variation must be observed. Suppose these variations are linear, then the ratio between the volume variation and pressure variation is always constant. This constant is called the compliance of the vessel and is given by

$$C = \frac{V - V_{us}}{p - p_{us}}, \quad (3.2)$$

where  $C$  is the compliance,  $V$  is the total volume after the vessel distention,  $V_{us}$  is the unstressed volume,  $p$  is the instantaneous blood pressure and  $p_{us}$  is the associated unstressed pressure. Adopting a null unstressed pressure, the pressure-volume relation can be formulated as

$$V = V_{us} + Cp. \quad (3.3)$$

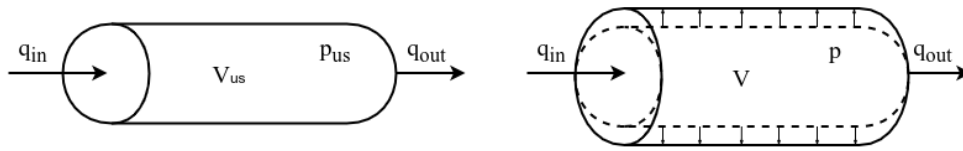
The vessel compliance is measured in *millilitres by millimetres* of mercury ( $ml/mmHg$ ) and its representation is analogous to that of a capacitor in an electrical circuit. It is also possible to introduce the idea of an elastance vessel (inverse of compliance), which given the assumed linear variations of volume and pressure, is expressed by

$$E = \frac{p - p_{us}}{V - V_{us}}, \quad (3.4)$$

where  $E$  is the elastance. Using this constant, the pressure-volume relation can be expressed as

$$V = V_{us} + E^{-1}p. \quad (3.5)$$

Figure 8 – A compliance vessel. In the left the compliance vessel is at its unstressed state and in the right the vessel is subjected to a nonzero pressure variation;  $V_{us}$ : unstressed volume;  $p_{us}$ : unstressed pressure;  $V$ : total volume after the vessel distention;  $p$ : instantaneous pressure.



Source: Elaborated by the author.

If we consider that a compliant vessel undergoes a change of volume at an instant of time  $t$ , such that its volume is given by  $V = V(t)$ , then the blood volume retained in the vessel is exactly equal to the volume variation it underwent. Thus, the rate of change in volume is equal to the difference between the inflows and outflows, that is:

$$\frac{dV}{dt} = q_{in} - q_{out}. \quad (3.6)$$

The assumption of linear variations of pressure and volume within a vascular vessel considered so far are convenient simplifications. However, they are not suitable if we take the pumping action of the heart into account. The cardiac valves regulate the pumping of blood by allowing it to flow from a compartment  $i$  to a compartment  $j$  if the pressure  $p_i$  at the compartment  $i$  is greater than or equal to the pressure  $p_j$  at the compartment  $j$ , that is, if  $p_i \geq p_j$ . Otherwise, the blood flow is denied in case  $p_i < p_j$ , by keeping the valve closed. Modeling the cardiac valves with this opening-closing mechanism is analogous to the representation of a diode in an electrical circuit since it ensures that blood will flow in only one direction (55).

Additionally, since the heart chambers are actively pumping blood, it is not suitable to model them as a compliance vessel with a constant compliance or elastance. Therefore, they should be regarded as a vessel whose compliance (or elastance) changes as a function of time. Adapting Equation (3.3), the pressure-volume relation for a heart chamber should be

$$V(t) = V_{us} + C(t)p(t), \quad (3.7)$$

or adapting Equation (3.5) it results in:

$$V(t) = V_{us} + E^{-1}(t)p(t), \quad (3.8)$$

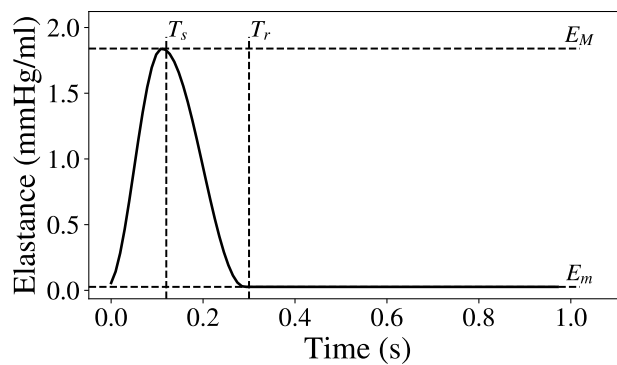
where  $C(t)$  and  $E(t)$  are time-varying compliance and elastance functions, respectively.

The models studied here are concerned with the systemic circulation and consider only the left heart (ventricle and atrium) function, out of the four chambers of the heart. The left heart pressure-volume relation, as expressed in Equation (3.8), was first presented by (59) and has been widely used in other studies (29, 55, 58, 33, 25). The time-varying elastance function provides the pumping mechanism of the heart chambers. Here, we present an elastance function for the left heart, based on (33), which has the following form:

$$E_{lh}(\tilde{t}) = \begin{cases} \frac{E_M - E_m}{2} \left( 1 - \cos\left(\frac{\pi\tilde{t}}{T_s}\right) \right) + E_m, & \tilde{t} \leq T_s \\ \frac{E_M - E_m}{2} \left( \cos\left(\frac{\pi(\tilde{t} - T_s)}{T_r - T_s}\right) + 1 \right) + E_m, & T_s \leq \tilde{t} \leq T_r \\ E_m, & T_r \leq \tilde{t} \leq T \end{cases} \quad (3.9)$$

where  $\tilde{t}$  is the time within a cardiac cycle. Maximum and minimum elastances are represented by the parameters  $E_M$  and  $E_m$ , respectively, while the times at which they occur are given by  $T_s$  and  $T_r$ , respectively. As depicted in Figure 9 the function reaches its maximum value  $E_M$  at time  $T_s$ , which is when systole ends, and the minimum value  $E_m$  is achieved at time  $T_r$ .

Figure 9 – Time-varying elastance function during a cardiac cycle;  $T_s$ : time of maximum elastance;  $T_r$ : time of minimum elastance;  $E_M$ : maximum elastance value;  $E_m$ : minimum elastance value.



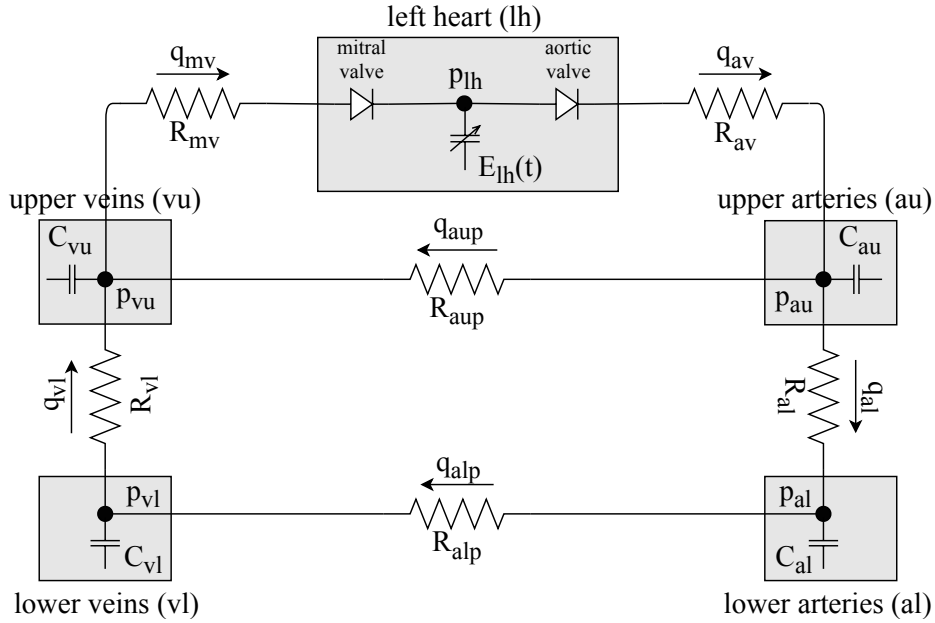
Source: Elaborated by the author.

### 3.2.1 Five-compartment model

The first model studied was a five-compartment LP model describing a closed-loop systemic circulation. This model was first presented in the work of (25) to examine cardiovascular

regulation during the head-up tilt (HUT) protocol. It considers the dynamics of the systemic circulation, taking into account the upper and lower body vessels and the left heart.

Figure 10 – Systemic circulation representation of the five-compartment model.



Source: Elaborated by the author.

In this model, equations for the pressure-volume relation in the systemic vessels are defined following Equation (3.3), that is

$$V_{au} = V_{au,us} + C_{au}p_{au}, \quad (3.10)$$

$$V_{al} = V_{al,us} + C_{al}p_{al}, \quad (3.11)$$

$$V_{vu} = V_{vu,us} + C_{vu}p_{vu}, \quad (3.12)$$

$$V_{vl} = V_{vl,us} + C_{vl}p_{vl}, \quad (3.13)$$

where the subscripts  $au$ ,  $al$ ,  $vu$ ,  $vl$  denote the upper and lower arteries and the upper and lower veins, respectively. The left heart compartment equation for the pressure-volume relation follows Equation (3.8), that is:

$$V_{lh}(t) = V_{lh,us} + E_{lh}^{-1}(t)p_{lh}(t), \quad (3.14)$$

where the subscript  $lh$  denotes the left heart and the time-varying elastance function  $E_{lh}(t)$  was defined in Equation (3.9).

Flows between upper and lower arteries ( $q_{al}$ ), lower and upper veins ( $q_{v1}$ ), and through upper and lower peripheral arteries ( $q_{aup}$  and  $q_{alp}$ , respectively) are modeled following Equa-

tion (3.1) for resistance vessels, that is:

$$q_{al} = \frac{p_{au} - p_{al}}{R_{al}}, \quad (3.15)$$

$$q_{vl} = \frac{p_{vl} - p_{vu}}{R_{vl}}, \quad (3.16)$$

$$q_{aup} = \frac{p_{au} - p_{vu}}{R_{aup}}, \quad (3.17)$$

$$q_{alp} = \frac{p_{al} - p_{vl}}{R_{alp}}. \quad (3.18)$$

Flow through the mitral and aortic valves ( $q_{mv}$  and  $q_{av}$ , respectively) must respect the opening-closing mechanism of the valves, that is:

$$q_{mv} = \begin{cases} \frac{p_{vu} - p_{lh}}{R_{mv}}, & p_{vu} \geq p_{lh} \\ 0, & p_{vu} < p_{lh} \end{cases} \quad (3.19)$$

$$q_{av} = \begin{cases} \frac{p_{lh} - p_{au}}{R_{av}}, & p_{lh} \geq p_{au} \\ 0, & p_{lh} < p_{au} \end{cases} \quad (3.20)$$

Finally, the rate of volume change in the compartments follows Equation (3.6) and is denoted by

$$\frac{dV_{au}}{dt} = q_{av} - (q_{aup} + q_{al}), \quad (3.21)$$

$$\frac{dV_{al}}{dt} = q_{al} - q_{alp}, \quad (3.22)$$

$$\frac{dV_{vu}}{dt} = (q_{vl} + q_{aup}) - q_{mv}, \quad (3.23)$$

$$\frac{dV_{vl}}{dt} = q_{alp} - q_{vl}, \quad (3.24)$$

$$\frac{dV_{lh}}{dt} = q_{mv} - q_{av}. \quad (3.25)$$

Section 3.3 describes models and numerical methods regarding the simulation of the coupled multi-scale model studied in this work. The model couples the FE simulation of the electromechanical activity of the left ventricle with the simulation of the systemic circulation performed with a LP model. Such multi-scale simulation can be costly, time-consuming, and difficult in terms of parameter calibration. Therefore, it is attractive to consider simpler models. Since our study is concerned with hemodynamic parameters regarding left ventricular volumes and global arterial pressures, a separation between upper and lower body dynamics as in the five-compartment model presented here is not necessary and therefore, a model simplification can be considered to reduce the parameter space and enhance the simulation.

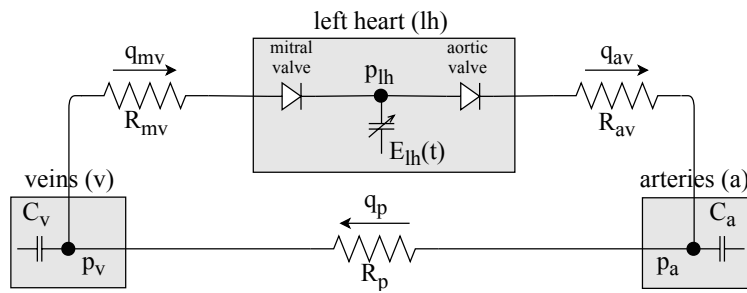
### 3.2.2 A reduced model

We present a possible simplification of the five-compartment model to a model with a reduced number of parameters. A possible procedure to reduce the model is to lump the lower

and upper body compartments together, as depicted by Figure 11. The sensitivity analysis for the five-compartment model presented in the next chapter will substantiate the model simplification considering the quantities of interest evaluated.

Equations applied for this 3-compartment model follow the same idea presented for the original model. The number of equations to be solved was reduced, whereas some parameters and initial conditions needed to be recalculated to reproduce the original model. Further considerations taken for the reduced model are presented next.

Figure 11 – Systemic circulation representation of the three-compartment model.



Source: Elaborated by the author.

The model is simplified by merging the lower and upper veins compartments into the veins compartment (subscript  $v$ ). The lower and upper arteries are combined into the arteries compartment (subscript  $a$ ), as seen in Figure 11. Parameters and initial conditions of the simplified model were adapted as follows.

Initial volume for the arteries compartment  $V_a$  is given by the sum of the initial volumes of the upper and lower body compartments from the original model. The same idea is applied for the volume  $V_v$  of the veins compartment. Thus, the initial volumes are given by:

$$V_a(0) = V_{al}(0) + V_{au}(0), \quad (3.26)$$

$$V_v(0) = V_{vl}(0) + V_{vu}(0). \quad (3.27)$$

Compliances are obtained with

$$C = \frac{\bar{V} - \bar{V}_{us}}{\bar{p}} = \frac{V_s}{\bar{p}}, \quad (3.28)$$

where  $C$  is the compliance and  $\bar{V}$ ,  $\bar{V}_{us}$ ,  $V_s$  and  $\bar{p}$  are mean values for volumes and pressures from the original five-compartment model (33). Thus, we approximated the compliances for the simplified model as follows

$$C_a = \frac{V_{au,s} + V_{al,s}}{\bar{p}_a}, \quad (3.29)$$

$$C_v = \frac{V_{vu,s} + V_{vl,s}}{\bar{p}_v}, \quad (3.30)$$

where  $\bar{p}_a = (\bar{p}_{au} + \bar{p}_{al})/2$  and  $\bar{p}_v = (\bar{p}_{vu} + \bar{p}_{vl})/2$ . The value of the peripheral resistance of the simplified model was also adapted. Resistances  $R_{vl}$ ,  $R_{al}$  and  $R_{alp}$  are in series, and the sum of them is in parallel with  $R_{aup}$ , as shown in Figure 10. Thus, we calculated the equivalent resistance  $R_p$  using the following expression:

$$\frac{1}{R_p} = \frac{1}{R_{alp} + R_{vl} + R_{al}} + \frac{1}{R_{aup}}. \quad (3.31)$$

Therefore, the equations for the pressure-volume relation for the three-compartment model are given by

$$V_a = V_{a,us} + C_a p_a, \quad (3.32)$$

$$V_v = V_{v,us} + C_v p_v, \quad (3.33)$$

$$V_{lh}(t) = V_{lh,us} + E_{lh}^{-1}(t) p_{lh}(t), \quad (3.34)$$

where  $V_a$ ,  $V_v$  and  $V_{lh}$  are the arterial, venous and left heart volumes, respectively, and the time-varying elastance function  $E_{lh}$  is defined in Equation (3.9). Peripheral flow  $q_p$ , and flows through the mitral valve  $q_{mv}$  and aortic valve  $q_{av}$  are given by

$$q_p = \frac{p_a - p_v}{R_p}, \quad (3.35)$$

$$q_{mv} = \begin{cases} \frac{p_v - p_{lh}}{R_{mv}}, & p_v \geq p_{lh} \\ 0, & p_v < p_{lh} \end{cases} \quad (3.36)$$

$$q_{av} = \begin{cases} \frac{p_{lh} - p_a}{R_{av}}, & p_{lh} \geq p_a \\ 0, & p_{lh} < p_a \end{cases} \quad (3.37)$$

Lastly, the rate of volume change in the compartments are given by

$$\frac{dV_a}{dt} = q_{av} - q_p, \quad (3.38)$$

$$\frac{dV_v}{dt} = q_p - q_{mv}, \quad (3.39)$$

$$\frac{dV_{lh}}{dt} = q_{mv} - q_{av}. \quad (3.40)$$

### 3.2.3 Numerical solution

The pulsatile nature of the models is characterized by the time-varying elastance curve and the opening and closing mechanism of the valves, which predicts flow into and out of the valves. Such a mechanism introduces discontinuity characterizing the system of differential equations as stiff (32), which in turn introduces numerical difficulties. When solving stiff problems, explicit methods perform poorly and require small time steps. Therefore, it is essential to consider appropriate methods for their solution.

The backward differentiation formula (BDF) methods (60, 61) are a class of methods capable of efficiently solving stiff problems. To solve the LP equations, we used the BDF method implemented in the SciPy (62) library of the Python programming language.

For both models, once the volumes are calculated by applying the BDF method on the equations for the rate of volume change (equations (3.21)-(3.25) for the 5-compartment model and equations (3.38)-(3.40) for the 3-compartment model), and using the appropriate flows  $q_{in}$  and  $q_{out}$ , pressure and flow are obtained. To compute them, equations for the pressure-volume relation are used (equations (3.10)-(3.14) for the 5-compartment model and equations (3.32)-(3.34) for the 3-compartment model) as well as the equations for the resistance vessel flows (equations (3.15)-(3.20) for the 5-compartment model and equations (3.35)-(3.37) for the 3-compartment model).

### 3.2.4 Five-compartment model simulation

Since the focus of this work is on UQ and SA for the LP and coupled models, we present here the results of simulating the five-compartment model using nominal values for the parameters reported in the literature. The parameters and initial conditions considered for the simulation of the five-compartment model are from the work of (33), which were obtained from experimental data and model fitting, considering a study of patient-specific dynamics during HUT. Table 4 shows all the parameter values and initial conditions used in the simulation.

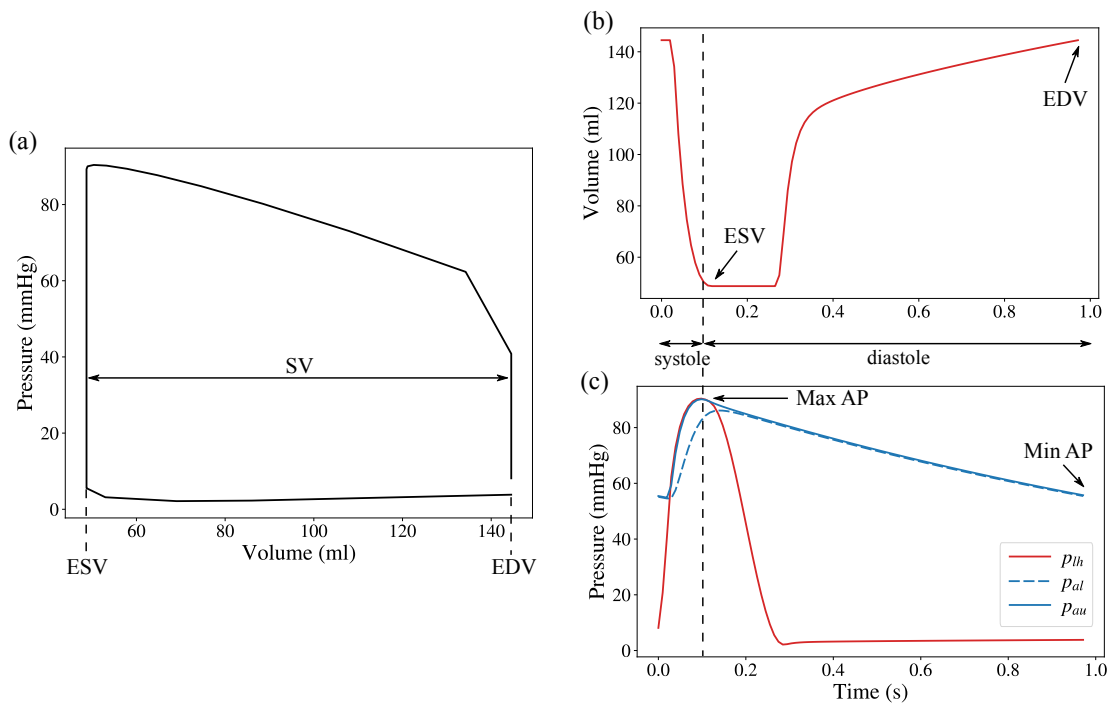
Table 4 – Five-compartment model: initial conditions and parameters.

Name	Description	Value	Units
<b>initial conditions</b>			
$V_{au,s}(0)$	Upper arterial initial volume	145.241	<i>ml</i>
$V_{al,s}(0)$	Lower arterial initial volume	25.631	<i>ml</i>
$V_{vu,s}(0)$	Upper venous initial volume	161.378	<i>ml</i>
$V_{vl,s}(0)$	Lower venous initial volume	28.479	<i>ml</i>
$V_{lh,s}(0)$	Left ventricle initial volume	132.000	<i>ml</i>
<b>parameters</b>			
$C_{au}$	Upper arterial compliance	2.1335	<i>ml/mmHg</i>
$C_{al}$	Lower arterial compliance	0.37649	<i>ml/mmHg</i>
$C_{vu}$	Upper venous compliance	46.108	<i>ml/mmHg</i>
$C_{vl}$	Lower venous compliance	7.5943	<i>ml/mmHg</i>
$E_M$	Maximal ventricular elastance value	1.8399	<i>mmHg/ml</i>
$E_m$	Minimum ventricular elastance value	0.026515	<i>mmHg/ml</i>
$R_{aup}$	Peripheral upper arterial resistance	0.86735	<i>mmHg s/ml</i>
$R_{alp}$	Peripheral lower arterial resistance	3.3828	<i>mmHg s/ml</i>
$R_{al}$	Lower arterial resistance	0.073149	<i>mmHg s/ml</i>
$R_{vl}$	Lower venous resistance	0.013431	<i>mmHg s/ml</i>
$R_{av}$	Aortic valve resistance	0.001	<i>mmHg s/ml</i>
$R_{mv}$	Mitral valve resistance	0.001	<i>mmHg s/ml</i>
$T$	Cardiac cycle duration	0.98	<i>s</i>
$T_s$	Time of maximum ventricular elastance	0.12	<i>s</i>
$T_r$	Time of minimum ventricular elastance	0.30	<i>s</i>

Source: Adapted from Williams *et al.* (2019).

The simulation performed considered 10 cardiac cycles with 100 time steps of size  $\Delta t = 0.0098 \text{ s}$ , producing cycles of 0.98 seconds. Figure 12 depicts the left heart pressure-volume loop, arterial pressure, left heart pressure, and volume during the last cardiac cycle. One can observe the systolic phase from 0 s to 0.12 s and the diastolic phase from 0.12 s to 0.98 s in the left heart pressure and volume curves. The results show physiologically consistent data for the left heart and arterial measures, which agree with those presented in (33). The figure also indicates the obtained hemodynamic parameters from the left heart (SV, EDV, ESV) and the arteries (Max AP and Min AP).

Figure 12 – Five-compartment model simulation results. (a) Pressure-volume loop for the last of 10 cardiac cycles; (b) Left heart volume during the last of 10 cardiac cycles; (c) Left heart and arterial pressures during the last of 10 cardiac cycles.



Source: Elaborated by the author.

Table 5 shows the hemodynamic values obtained with the simulation of the model. ESV, EDV, SV, EF, Max AP and Min AP quantities were calculated using the data from the last cycle of the simulation.

Table 5 – Hemodynamic values obtained in the simulations of the 5-compartment model.

ESV [ml]	EDV [ml]	SV [ml]	EF [%]	Max AP [mmHg]	Min AP [mmHg]
48.74	144.50	95.76	66.27	90.19	54.86

Source: Elaborated by the author.

### 3.2.5 Three-compartment model simulation

To maintain a similar qualitative and quantitative response to the five-compartment model, the reduced three-compartment model considered the same initial conditions and parameters when possible, and applied the adaptations described previously when necessary. Table 6 shows the parameters and initial condition values used.

Table 6 – Three-compartment model: initial conditions and parameters.

Name	Description	Value	Units
<b>initial conditions</b>			
$V_{a,s}(0)$	Arterial initial volume	170.872	<i>ml</i>
$V_{v,s}(0)$	Venous initial volume	189.857	<i>ml</i>
$V_{lh,s}(0)$	Left heart initial volume	132.000	<i>ml</i>
<b>parameters</b>			
$C_a$	Arterial compliance	2.50985	<i>ml/mmHg</i>
$C_v$	Venous compliance	54.2446	<i>ml/mmHg</i>
$E_M$	Maximal left heart elastance value	1.8399	<i>mmHg/ml</i>
$E_m$	Minimum left heart elastance value	0.026515	<i>mmHg/ml</i>
$R_p$	Peripheral arterial resistance	0.69384	<i>mmHg s/ml</i>
$R_{av}$	Aortic valve resistance	0.001	<i>mmHg s/ml</i>
$R_{mv}$	Mitral valve resistance	0.001	<i>mmHg s/ml</i>
$T$	Cardiac cycle duration	0.98	<i>s</i>
$T_s$	Time of maximum left heart elastance	0.12	<i>s</i>
$T_r$	Time of minimum left heart elastance	0.30	<i>s</i>

Source: Elaborated by the author.

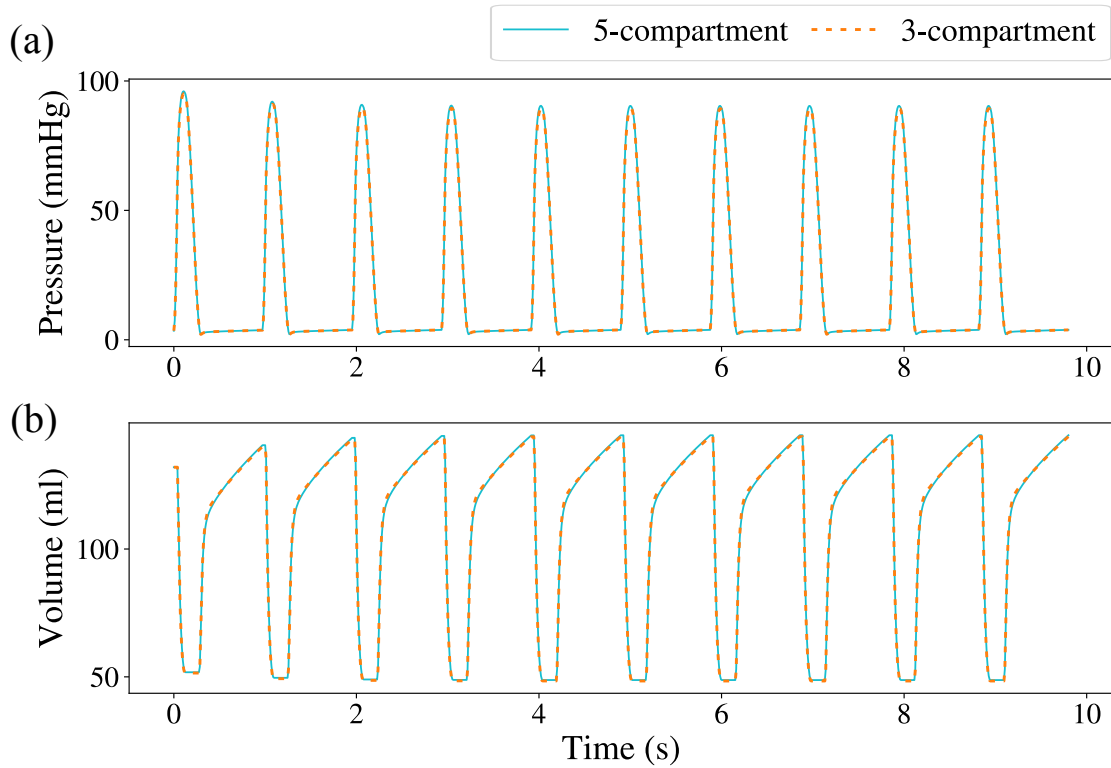
The simulation considered the same settings provided for the five-compartment model simulation, that is: 10 cardiac cycles, each with 100 time steps of size  $\Delta t = 0.0098$  s. The results of the three-compartment model are very similar and, therefore not presented. A comparison between the five and three-compartment models is presented in Figure 13, which shows the pressure and volume of the left heart during 10 cardiac cycles in both models. The results show that the simplified model responds very closely to the five-compartment model for this experiment. Within all cycles, solutions for the left ventricle pressure and volume showed a relative error of about 0.011 and 0.006, respectively.

Lastly, Table 7 compares the obtained hemodynamic parameters by the five-compartment and three-compartment model. One can see that the values are very close, confirming that the reduced model was able to predict similar LV hemodynamics of the original model under the conditions considered in the present work.

### 3.3 COUPLED MODEL

The multi-scale model studied in this work is presented here. Following, the details of the mechanical problem to be solved by the FE model, as well as the approach used to perform

Figure 13 – Comparison between the two models for a simulation of 9.8 s. (a) Left heart pressure. (b) Left heart volume.



Source: Elaborated by the author.

Table 7 – Comparison between values obtained in the simulations of the models.

Hemodynamic Value	5-compartment model	3-compartment model
ESV [ml]	48.74	48.38
EDV [ml]	144.50	143.96
SV [ml]	95.76	95.58
EF [%]	66.27	66.39
Max AP [mmHg]	90.19	89.16
Min AP [mmHg]	54.86	54.92

Source: Elaborated by the author.

the coupling of the LP model and the FE element model, are described.

### 3.3.1 Cardiac tissue mechanics model

The modeling of cardiac tissue mechanics is based on fundamental concepts of continuum mechanics, which will be only briefly presented here for a detailed presentation and discussion see (63, 15, 64). From the principle of linear conservation of momentum, the equations of force equilibrium can be derived. Neglecting inertial effects, the governing equations used to describe

the cardiac tissue deformation results in the following problem: find the displacement field  $\mathbf{u}$ , such that

$$\left\{ \begin{array}{ll} \nabla \cdot (\mathbf{FS}) + \mathbf{B} = 0, & \text{in } \Omega_0, \\ \mathbf{u} = \bar{\mathbf{u}}, & \text{on } \partial\Omega_0^D, \\ \mathbf{FSN} = \bar{\mathbf{T}}, & \text{on } \partial\Omega_0^N. \end{array} \right. \quad (3.41)$$

where  $\Omega_0$  is the reference configuration,  $\bar{\mathbf{u}}$  are the prescribed displacements on the boundary  $\partial\Omega_0^D$  and  $\bar{\mathbf{T}}$  is the traction applied on the boundary  $\partial\Omega_0^N$ , with a normal vector  $\mathbf{N}$ . The strain gradient tensor is given by  $\mathbf{F}$ ,  $\mathbf{S}$  is the second tensor of Piola-Kirchhoff and  $\mathbf{B}$  are the body forces.

The cardiac tissue is composed of muscle fibers that are bundled in sheets of parallel fibers. The complex microstructural organization of the cardiac tissue results in an anisotropic mechanical response. Constitutive models attempt to describe this anisotropic behaviour, in which, the stiffness is greater in the fiber direction than in other directions (65, 66, 67). The constitutive model for the cardiac tissue used is the one proposed by (67), in which the strain function is given by

$$\Psi = \frac{c}{2}(e^Q - 1), \quad (3.42)$$

with

$$Q = b_f E_{11}^2 + b_t (E_{22}^2 + E_{33}^2 + E_{23}^2 + E_{32}^2) + b_{fs} (E_{12}^2 + E_{21}^2 + E_{13}^2 + E_{31}^2), \quad (3.43)$$

where  $c$ ,  $b_f$ ,  $b_t$  and  $b_{fs}$  are material related parameters and  $E_{ij}$  are the Green-Lagrange strain tensor components.

### 3.3.2 Active stress

The active force generated at the cellular level is responsible for the contraction of cardiac myocyte, which when combined results in cardiac tissue contraction. To model the effects of contraction, the mechanical problem must take the active force in consideration. One way to model (68) is to split the second Piola-Kirchhoff stress tensor in a passive component  $\mathbf{S}_p$  and an active component  $\mathbf{S}_a$ , thus

$$\mathbf{S} = \mathbf{S}_p + \mathbf{S}_a, \quad (3.44)$$

where the passive component describes the passive behaviour of the heart and is derived from the constitutive model (Equation (3.42)), while the active part is given by:

$$\mathbf{S}_a = T_{ref} T_a \mathbf{f} \otimes \mathbf{f}, \quad (3.45)$$

where  $T_a$  is the normalized active stress generated by a cellular electro-mechanical model (26, 69, 70),  $T_{ref}$  is a reference value for the stress and  $\mathbf{f}$  defines the fiber direction in the undeformed configuration.

To generate the active stress  $T_a$  as in Equation (3.45), the model presented by (69) is used here. In this approach, the magnitude of  $T_a$  depends on the time elapsed since activation of

a cell membrane  $t_a$ , sarcomere length  $l_s$ , and contractile element length  $l_c$ :

$$T_a = \frac{l_s}{l_{s0}} f_{iso}(l_c) f_{twitch}(t_a, l_s) E_a (l_s - l_c), \quad (3.46)$$

where  $l_{s0}$  is the sarcomere length in the stress-free state and  $E_a$  is the stiffness of the elastic element. The function  $f_{iso}$  describes the isometric stress as follows

$$f_{iso}(l_c) = \begin{cases} T_0 \tanh^2 [a_l (l_c - l_{c0})], & l_c \geq l_{c0} \\ 0, & l_c < l_{c0} \end{cases} \quad (3.47)$$

where  $T_0$  is a reference active stress level,  $a_l$  is responsible for the steepness of the stress-length curve,  $l_{c0}$  is the contractile element length when the active stress is zero. The myofiber stress time dependence function  $f_{twitch}$  is given by

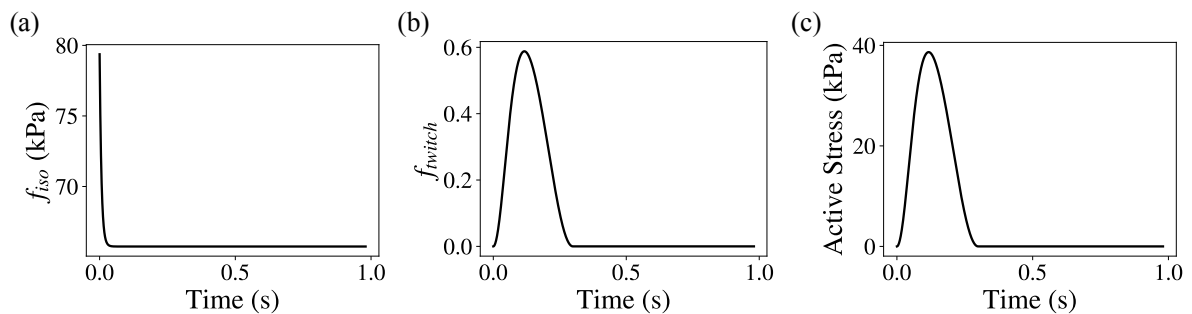
$$f_{twitch}(t_a, l_s) = \begin{cases} 0, & 0 > t_a \\ \tanh^2 \left( \frac{t_a}{\tau_r} \right) \tanh^2 \left( \frac{t_{max} - t_a}{\tau_d} \right), & 0 \leq t_a \leq t_{max} \\ 0, & t_a > t_{max} \end{cases} \quad (3.48)$$

where  $t_{max} = b(l_s - l_d)$  is the twitch duration,  $\tau_r$  and  $\tau_d$  govern the rise and decay time of the twitch, respectively,  $b$  is the increase of twitch duration with sarcomere length, and  $l_d$  is the sarcomere length where twitch duration is zero. The time course of the contractile element  $l_c$  follows the first order differential equation

$$\frac{dl_c}{dt} = [E_a (l_s - l_c) - 1] v_0, \quad (3.49)$$

where  $v_0$  is the unloaded shortening velocity. Figure 14 illustrates the active stress curve, as well as the behaviour of the  $f_{iso}$  and  $f_{twitch}$  functions over the course of cardiac cycle of 0.98 seconds.

Figure 14 – Active stress curve during a full cardiac cycle. (a) The  $f_{iso}$  function; (b) The  $f_{twitch}$  function; (c) Active stress curve.



Source: Elaborated by the author.

### 3.3.3 Models coupling

Given all the concepts and models related to cardiac tissue mechanics, along with the active stress approach presented, the procedure used to couple the three-compartment LP model

and the FE model can now be explained. The method of ventricular-vascular coupling used here is based on the method proposed by (71) in which ventricular cavity pressures are estimated until convergence is achieved. The blood volume in the ventricular cavity provided by the LP model cannot be used as a boundary condition when solving the FE mechanics model. Therefore the procedure is to estimate new cavity pressures based on the minimized cavity volume differences between the LP model and FE model predictions. Hemodynamic coupling is achieved by attending the scheme represented by the flowchart in Figure 15. Next, we present the coupling procedure of (71) in a simplified way, which accounts for the left ventricle only, whereas the original method works for biventricular simulations.

For each timestep  $t$ , multiple estimations  $i$  are made for the ventricular cavity pressure. The first stage of the procedure consists of an initial estimation  $p_{LV,i}^{t+1}$  using the fourth order Adams-Bashforth scheme (60), that is

$$p_{LV,i}^{t+1} = p_{LV,i}^t + \frac{\Delta t}{24} (55f^t - 59f^{t-1} + 37f^{t-2} - 9f^{t-3}), \quad (3.50)$$

where  $f^t$  denotes the time derivative of the pressure for the timestep  $t$ , approximated by

$$f^t = \frac{p_{LV,i}^t - p_{LV,i}^{t-1}}{\Delta t}. \quad (3.51)$$

Since at the initial timesteps there are no previous knowledge of the pressure, a simple perturbation is applied to perform the estimation (71):

$$p_{LV,i}^{t+1} = p_{LV,i}^t + \varepsilon \Delta t, \quad (3.52)$$

where  $\varepsilon = 0.005$  is the perturbation value.

The ventricular cavity pressure estimation  $p_{LV,i}^{t+1}$  calculated is prescribed as boundary condition to solve the mechanics problem (3.41), which yields a ventricular cavity volume  $V_{LV,i,FE}^{t+1}$ . At the same time, the LP model computes the volume  $V_{LV,i,LP}^{t+1}$  using the mid-point method (60). First, fluxes are computed as

$$q_{p,i}^{t+\frac{1}{2}} = \frac{1}{2R_p} (p_{a,i-1}^{t+1} + p_a^t - p_{v,i-1}^{t+1} - p_v^t), \quad (3.53)$$

$$q_{mv,i}^{t+\frac{1}{2}} = \frac{1}{2R_{mv}} (p_{v,i-1}^{t+1} + p_v^t - p_{LV,i-1}^{t+1} - p_{LV}^t), \quad (3.54)$$

$$q_{ao,i}^{t+\frac{1}{2}} = \frac{1}{2R_{ao}} (p_{LV,i-1}^{t+1} + p_{LV}^t - p_{a,i-1}^{t+1} - p_a^t). \quad (3.55)$$

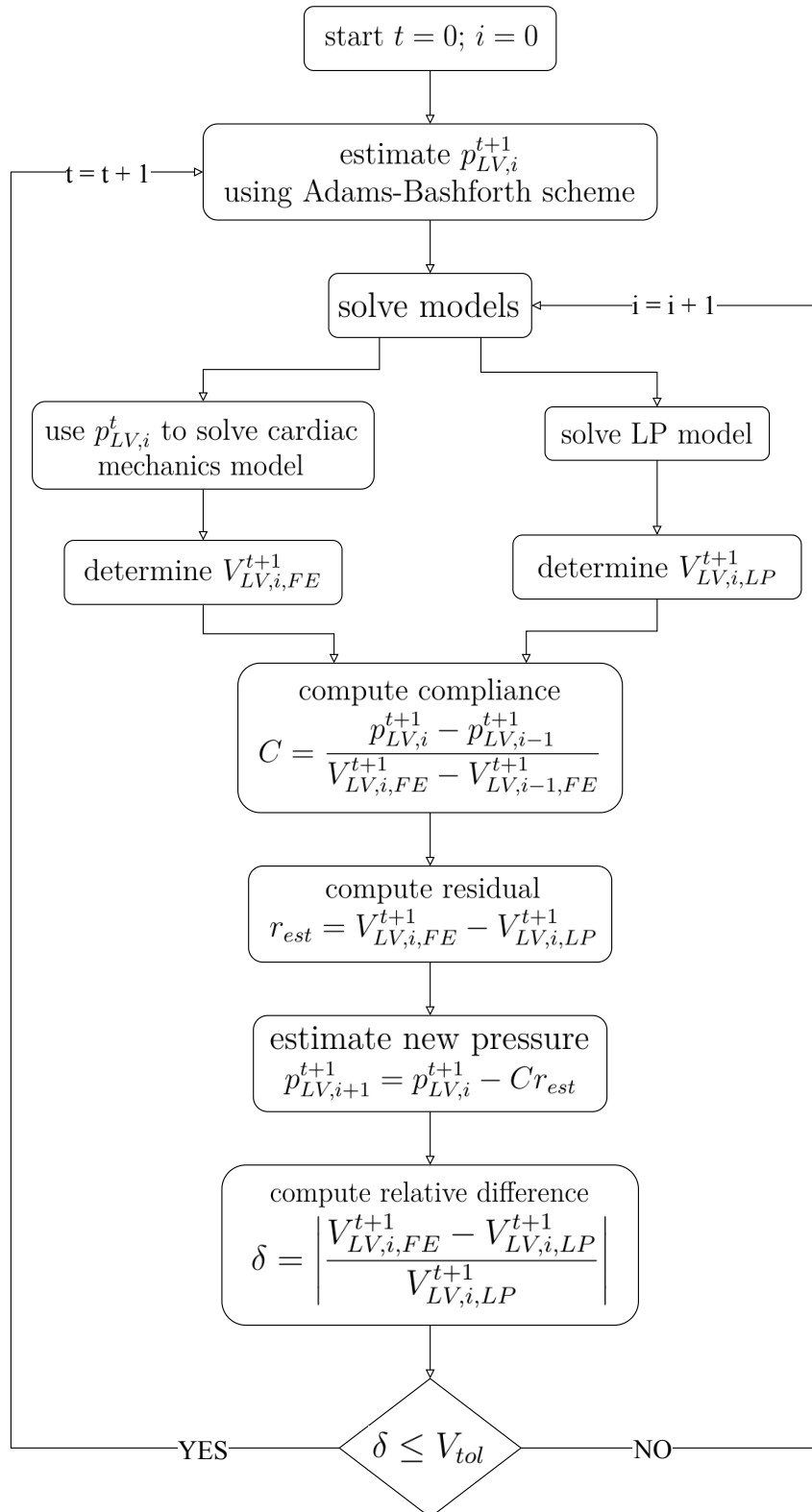
and then using Equation-(3.25) the left ventricular volume is updated. A new pressure estimation  $p_{LV,i+1}^{t+1}$  is computed as:

$$p_{LV,i+1}^{t+1} = p_{LV,i}^{t+1} - Cr_{est}, \quad (3.56)$$

where the compliance  $C$  is calculated using the previous estimates of the pressures (from steps  $i$  and  $i-1$ ) and volumes provided by the LP and FE models ( $V_{LV,i,LP}^{t+1}$  and  $V_{LV,i,FE}^{t+1}$ , respectively), that is

$$C = \frac{p_{LV,i}^{t+1} - p_{LV,i-1}^{t+1}}{V_{LV,i,FE}^{t+1} - V_{LV,i-1,FE}^{t+1}}, \quad (3.57)$$

Figure 15 – Flowchart of the iterative coupling scheme between the LP and FE models.



Source: Elaborated by the author.

and  $r_{est}$  is the estimation residual given by the difference between the cavity volume provided by the LP and FE models:

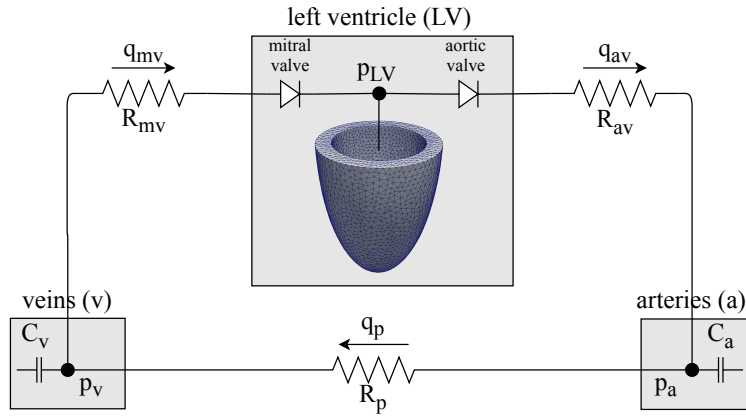
$$r_{est} = V_{LV,i,FE}^{t+1} - V_{LV,i,LP}^{t+1}. \quad (3.58)$$

After each new estimation step  $i$ , this residual should be reduced, until the relative volume difference given by

$$\delta = \left| \frac{V_{LV,i,FE}^{t+1} - V_{LV,i,LP}^{t+1}}{V_{LV,i,LP}^{t+1}} \right| \quad (3.59)$$

becomes smaller than a given tolerance  $V_{tol}$ . Figure 16 shows a diagram of the coupled FE and LP model.

Figure 16 – Systemic circulation representation of the coupled model.



Source: Elaborated by the author.

### 3.3.4 Numerical solution of the coupled model

The ventricular tissue contraction problem given by Equation (3.41) is solved with the *in-house* FE simulator *Cardiax*, which employs a mixed finite element formulation and the Augmented Lagrangian formulation (ALG) approach (64). The FE method uses a  $Q1 - Q0 - Q0$  scheme, where displacement is approximated with linear polynomials, whereas dilation and pressure are treated as constants at the element level (64). The discretization of this problem results in a non-linear system of equations, which is solved by Newton's method (72, 73). Then, a preconditioned iterative method based on an algebraic multigrid (AMG) preconditioner (73) is applied for the numerical solution of the resulting linear systems (15, 64).

### 3.3.5 Coupled model simulation

The simulation of the coupled model considered the same parameters of the three-compartment model for the systemic circulation, while the constitutive mechanics parameters

(Equations (3.42) and (3.43)) are adapted from the work of (15). The active stress curve applied to model the cellular contraction was obtained from the mathematical model presented by (26). The values used for the initial conditions, as well as parameters of the systemic circulation, mechanical problem, and the active stress models are shown in Table 8.

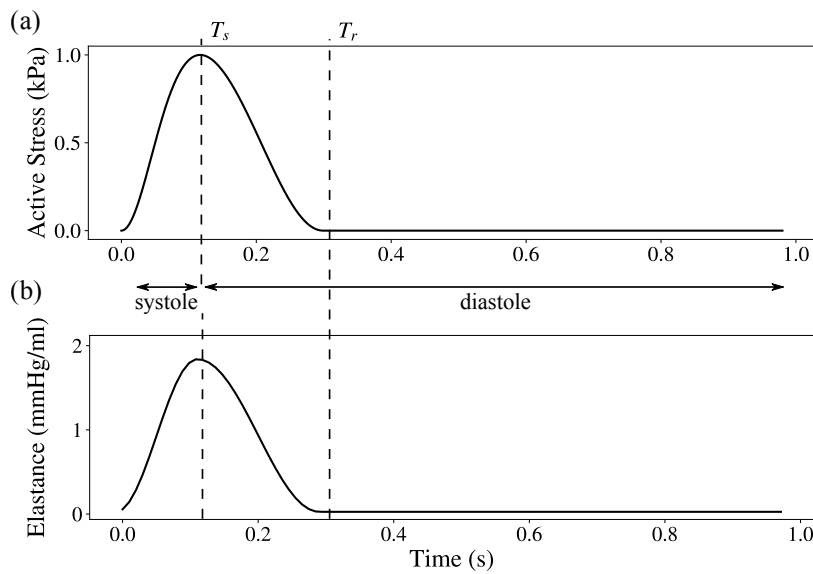
Table 8 – Coupled model: initial conditions and parameters.

Name	Description	Value	Units
<b>initial conditions</b>			
$p_a(0)$	Arterial initial pressure	68.08	<i>mmHg</i>
$p_v(0)$	Venous initial pressure	3.50	<i>mmHg</i>
$p_{LV}(0)$	Left ventricle initial pressure	0	<i>mmHg</i>
<b>circulatory parameters</b>			
$V_{a,us}$	Unstressed arterial volume	778.41	<i>ml</i>
$V_{v,us}$	Unstressed venous volume	3607.26	<i>ml</i>
$C_a$	Arterial compliance	2.50985	<i>ml/mmHg</i>
$C_v$	Venous compliance	54.2446	<i>ml/mmHg</i>
$E_M$	Maximal ventricular elastance value	1.8399	<i>mmHg/ml</i>
$E_m$	Minimum ventricular elastance value	0.026515	<i>mmHg/ml</i>
$R_p$	Peripheral arterial resistance	0.69384	<i>mmHg s/ml</i>
$R_{av}$	Aortic valve resistance	0.001	<i>mmHg s/ml</i>
$R_{mv}$	Mitral valve resistance	0.001	<i>mmHg s/ml</i>
$T$	Cardiac cycle duration	0.98	<i>s</i>
$T_s$	Time of maximum ventricular elastance	0.12	<i>s</i>
$T_r$	Time of minimum ventricular elastance	0.30	<i>s</i>
<b>mechanical problem parameters (adapted from (15))</b>			
$c$	Stress scale	6.38	<i>kPa</i>
$b_f$	Stiffness related parameter	6.63	
$b_t$	Stiffness related parameter	3.65	
$b_{fs}$	Stiffness related parameter	2.65	
$\kappa$	Bulk modulus	100	<i>kPa</i>
<b>active stress parameters (adapted from (26))</b>			
$a_l$	Stress-length curve steepness	2.0	$\mu m^{-1}$
$l_{c0}$	Contractile element length below 0	1.5	$\mu m$
$T_0$	Reference active stress	180.0	<i>kPa</i>
$E_a$	Elastic element stiffness	20.0	$\mu m^{-1}$
$v_0$	Shortening velocity	7.5	$\mu m s^{-1}$
$l_{s0}$	Sarcomere reference length	1.9	$\mu m$
$\tau_r$	Twitch rise constant	0.075	<i>s</i>
$\tau_d$	Twitch decay constant	0.150	<i>s</i>
$b$	Twitch duration increase	0.13	$s \mu m^{-1}$
$l_d$	Sarcomere length below 0	-0.4	$\mu m$
$T_{ref}$	Maximum active stress	65	<i>kPa</i>

Source: Elaborated by the author.

The simulation considered 1 cardiac cycle of 0.98 seconds divided in timesteps with a length of  $\Delta t = 0.0005$ . The input left ventricular FE mesh is a three-dimensional mesh comprised of 5752 nodes and 21609 tetrahedral elements. The active stress curve, as shown in Figure 17, was adjusted so that the times of maximum and minimum active stress values coincide with the times of maximum and minimum elastance ( $T_s$  and  $T_r$ , respectively) of the time-varying elastance function of Equation (3.9).

Figure 17 – Active stress and elastance curves for a cardiac cycle of 0.98 s. (a) Normalized active stress curve; (b) Time-varying elastance curve.

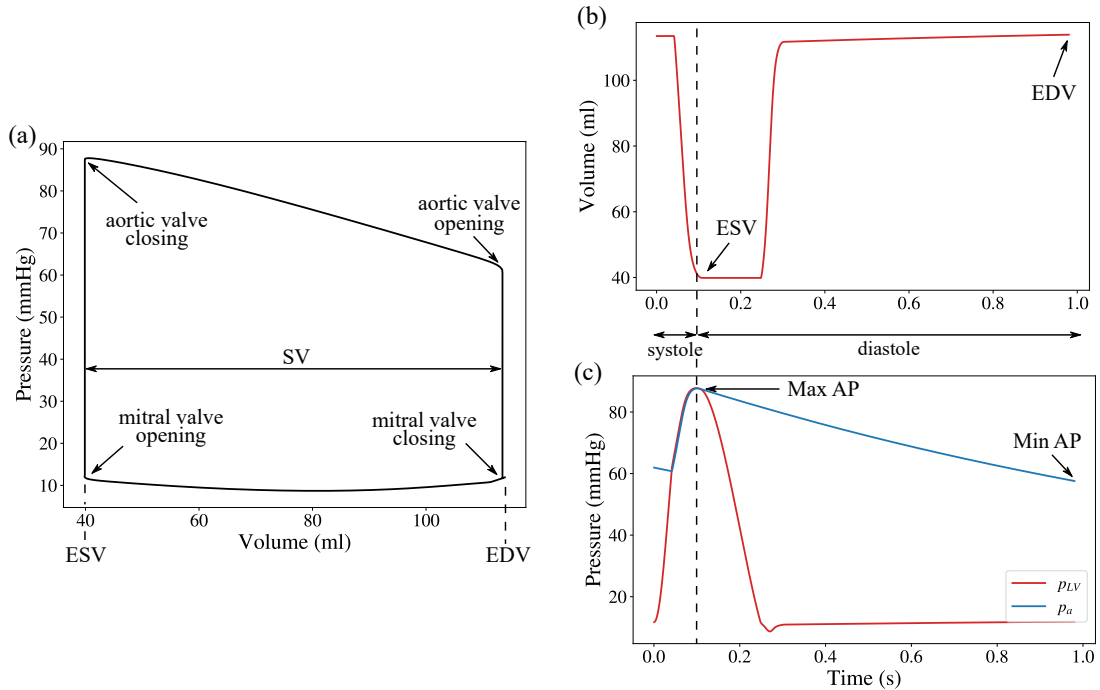


Source: Elaborated by the author.

Results shown in Figure 18 depicts the left ventricular pressure-volume loop, along with the arterial pressure and left ventricle pressure and volume. By comparing these results with the five-compartment results shown in Figure 12, it is possible to observe the desired similar qualitative behavior between the models. The systolic phase occurs from 0 s to 0.12 s and the diastolic phase from 0.12 s to 0.98 s, as shown in the left ventricular volume and pressure curves. Though slightly different from the LP models, results also show reasonable physiological responses for the left ventricular and arterial measures. The obtained hemodynamic parameters from the left ventricle (SV, EDV, ESV) and the arteries (Max AP and Min AP) are presented in Figure 18.

To show left ventricular behavior during a whole cardiac cycle, Figure 19 depicts the FE mesh at the beginning of each of the four phases of the left ventricular pressure-volume loop. At the beginning of the cycle (a), all valves are closed, and systole is at the beginning, representing that the left ventricle is filled and contraction leads to a rapid isovolumetric increase of pressure. The next phase (b) begins with the aortic valve opening, and the left ventricle ejects

Figure 18 – Coupled model simulation results. (a) Pressure-volume loop for the last of 3 cardiac cycles; (b) Left ventricle volume during the last of 3 cardiac cycles; (c) Left ventricle and arterial pressures during the last of 3 cardiac cycles.



Source: Elaborated by the author.

blood into the aorta until the end of the systole. After that, diastole begins (c) with the closing of the aortic valve, the left ventricle starts to relax, leading to an isovolumetric decay of pressure. Finally, when the mitral valve opens (d) the ventricle starts to fill again until the end of diastole is reached, completing the cycle.

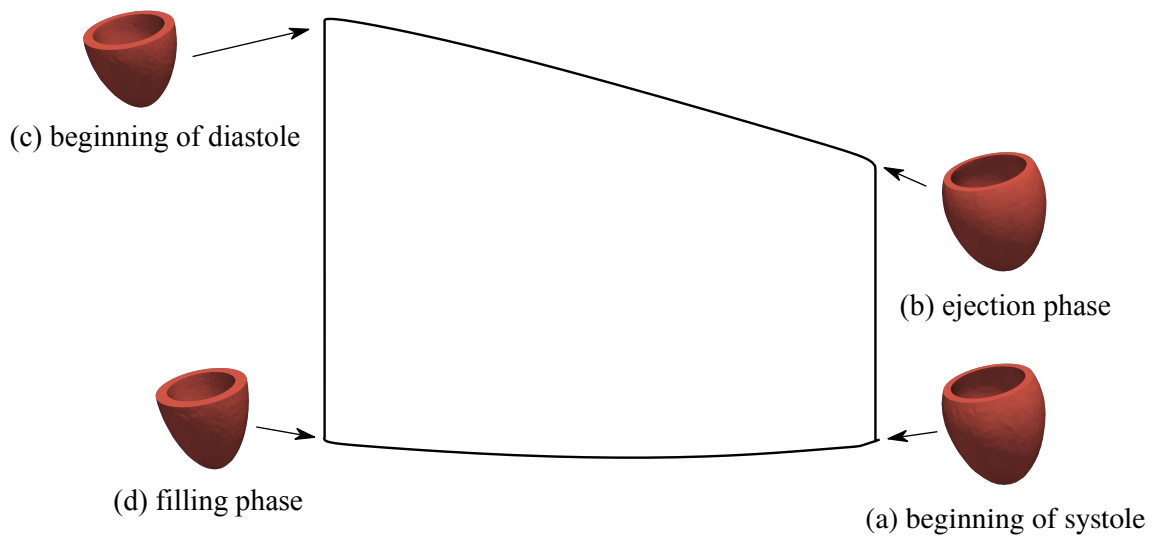
Table 9 shows the hemodynamic values obtained with the simulation of the coupled model, which shows a response within typical physiological ranges.

Table 9 – Hemodynamic values obtained in the simulations of the coupled.

EDV [ml]	ESV [ml]	SV [ml]	EF [%]	Max AP [mmHg]	Min AP [mmHg]
39.82	113.88	74.06	65.03	87.65	57.58

Source: Elaborated by the author.

Figure 19 – Left ventricle during the cardiac cycle. (a) Isovolumetric contraction phase (beginning of systole); (b) Ejection phase; (c) Isovolumetric relaxation (beginning of diastole); (d) Filling phase.



Source: Elaborated by the author.

## 4 RESULTS

In this chapter the results of UQ and SA studies performed in the LP and coupled models are presented. The goal is to analyze how the propagation of uncertainties from the input parameters of the model impacts on simulated measures of clinical interest. Six left ventricle hemodynamic quantities (Tables 3, 5 and 9) of common interest in clinical settings are considered as outputs of interest, that is: ESV, EDV, SV, EF, maximum AP, and minimum AP.

In this sense, we choose the sets of uncertain inputs and their configuration in such a way that the analyses can be done parsimoniously and objectively. We investigate those inputs of greater influence and that deserve to be measured with more precision (input prioritization), as well as those whose uncertainty has little impact when interact with others (input fixing).

### 4.1 ANALYSIS OF THE FIVE-COMPARTMENT MODEL

To carry out UQ and SA analyses we begin by defining the set of uncertain parameters for the five-compartment model. We regarded the parameters related to the elastance function (3.9), the resistances and the compliances as uncertain inputs. That is, the vector of uncertain inputs is given by:

$$\mathbf{Z}_5 = \{R_{aup}, R_{alp}, R_{al}, R_{vl}, R_{mv}, R_{av}, C_{au}, C_{al}, C_{vu}, C_{vl}, E_M, E_m, T_s, T_r\}. \quad (4.1)$$

Since we have no previous information about the distribution of these inputs, neither available experimental data, we set all parameters with a normal distribution with a coefficient of variation of 20% around their baseline values (from Tables 4).

The polynomial expansion in Equation (2.14) was constructed with order  $p = 2$  and a multiplicative factor  $m = 4$ , resulting in a total of  $N_s = 480$  samples. The calibration of the surrogate model shows that the determination coefficient (Equation (2.26)) was close to one for all QoIs, see Table 10. Therefore, we considered this choice of the polynomial degree  $p$  and multiplicative factor  $m$  in the following studies. Table 10 shows the determination coefficient obtained for different combinations of  $p$  and  $m$ . Table 10 shows that for  $p = 2$  and  $m = 4$  a reasonable accuracy is obtained at a moderate computational cost of performing 480 forward simulations to construct the surrogate model. Larger values for  $p$  or  $m$  can further increase the accuracy, but with a high computational cost.

#### 4.1.1 UQ and SA results

Uncertainty metrics calculated are presented in Table 11 for the scalar QoIs and in Figure 20 for the left heart pressure and volume as a time series. The ESV showed a significant variability (CoV=23%), whereas the others showed a moderate variability. The EF was the QoI that presented less variability, about 8% for the coefficient of variation. Figure 20 shows that the

Table 10 – LOO accuracy for each QoI of the 5-compartment model.

Factor $m$	Order $p$	Samples $N_s$	$Q^2$					
			ESV	EDV	SV	EF	MaxAP	MinAP
1	1	15	0.9635	0.4814	0.5179	0.9959	0.0905	0.7625
2	1	30	0.8868	0.7614	0.8007	0.9995	0.9146	0.9250
3	1	45	0.9061	0.8134	0.8456	0.9996	0.8901	0.9356
4	1	60	0.8493	0.8307	0.8743	0.9995	0.8783	0.9003
1	2	120	0.7212	0.8629	0.6002	0.9989	0.7837	0.9208
2	2	240	0.9393	0.9578	0.9486	0.9998	0.9557	0.9712
3	2	360	0.9736	0.9572	0.9563	0.9999	0.9556	0.9703
<b>4</b>	<b>2</b>	<b>480</b>	<b>0.9690</b>	<b>0.9655</b>	<b>0.9641</b>	<b>0.9999</b>	<b>0.9661</b>	<b>0.9759</b>

Source: Elaborated by the author.

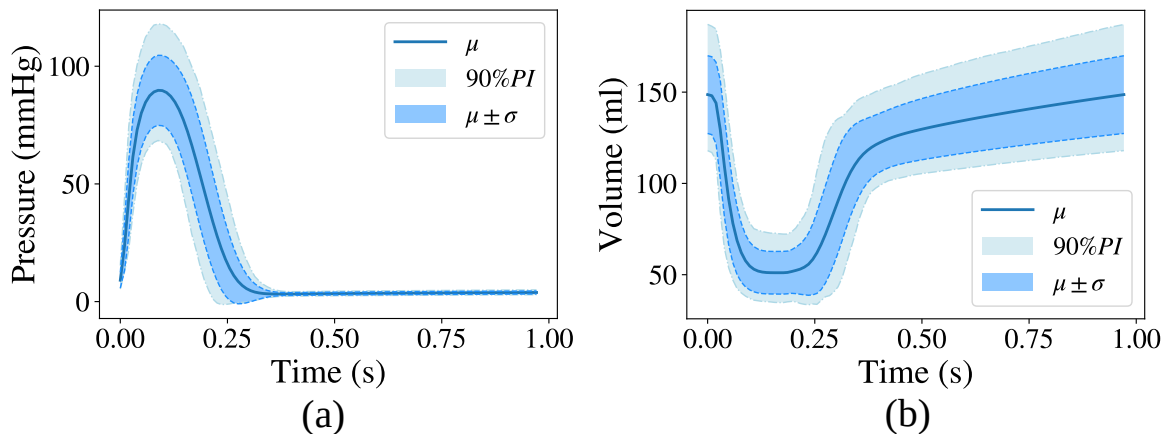
left heart pressure has a significant variance during the systole, around the period of maximum elastance at  $t = 0.12$  seconds, and during the beginning of diastole for  $t \leq 0.3$ , until it reaches its minimum value and maintains a small variance. The LV volume presents an opposite behavior: a significant variance is observed during the ventricular filling for  $t > 0.3$  seconds.

Table 11 – Uncertainty measures of each QoI for the 5-compartment model.

QoI	$\mu[Y]$	$\sigma[Y]$	CoV[Y]	90% PI
ESV [ml]	50.95	11.62	0.23	[35.04, 72.70]
EDV [ml]	148.64	21.28	0.14	[117.97, 187.04]
SV [ml]	97.69	16.60	0.17	[73.78, 128.62]
EF [-]	0.66	0.06	0.08	[55.56, 74.51]
MaxAP [mmHg]	91.06	14.80	0.16	[69.53, 119.22]
MinAP [mmHg]	53.46	9.17	0.17	[38.28, 69.11]

Source: Elaborated by the author.

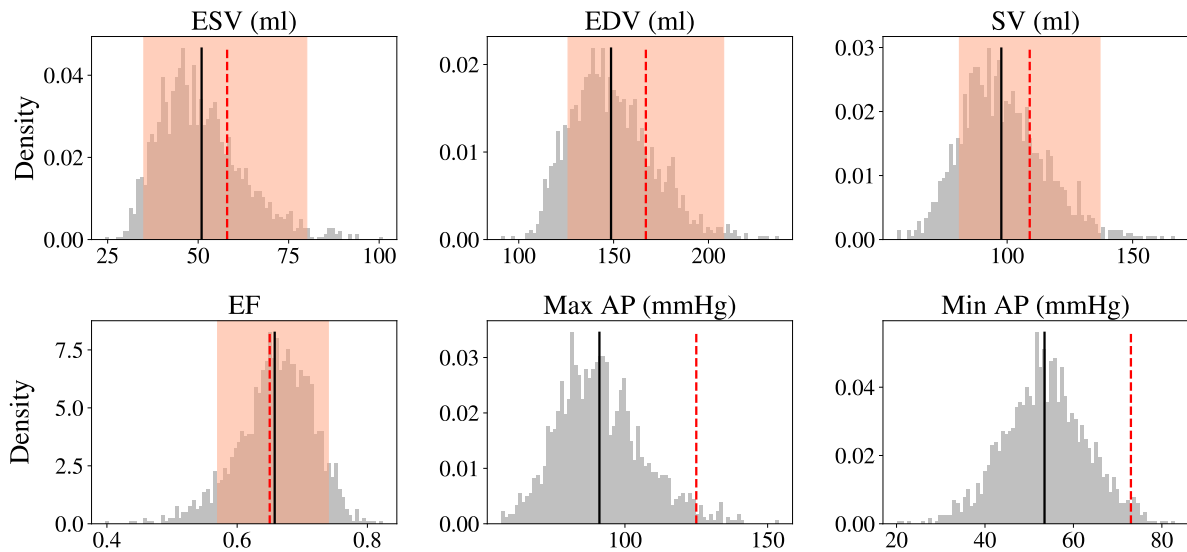
Figure 20 – Uncertainty propagation in the 5-compartment model for left ventricular pressure and volume; (a) pressure; and (b) volume.



Source: Elaborated by the author.

Figure 21 shows the evaluation of each QoI probability density function and reference values from the literature (74). It is possible to note that EDV, SV, Max AP, and Min AP present more symmetrical densities when compared to ESV and EF, which are more asymmetrical. Mean values from the literature (74) for a healthy male young adult (between 20 and 29 years old) are shown for all QoIs, together with the 95% confidence interval of the same type of subject for the ESV, EDV, SV, and EF. One can observe that the mean values of the 5-compartment model for ESV, EDV, SD, and EF are close to the values reported for a normal male adult (74). Values obtained for maximum and minimum pressure are lower than the reference values reported by (74), which does not report the 95% confidence interval for the systolic and diastolic blood pressures.

Figure 21 – Evaluated distribution of each scalar QoI for the 5-compartment model. The thick black line is the mean value obtained with UQ; the red dashed line is the mean value for a male young adult (74); the light red area is the 95% confidence interval for a male young adult (74).



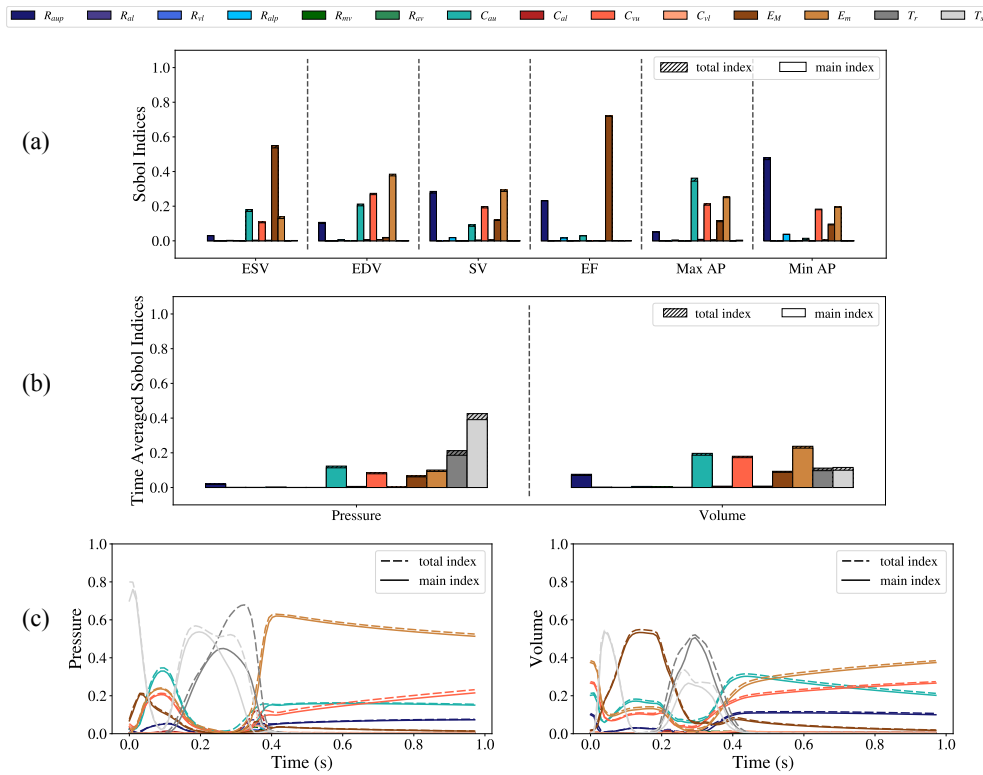
Source: Elaborated by the author.

Figure 22(a) shows the Sobol sensitivity indices for the output quantities. The results show that ESV and EF are profoundly impacted by the maximum elastance  $E_M$  parameter, whereas EDV and SV are impacted by the minimum elastance  $E_m$  parameter. The Max AP is highly impacted by the upper arterial compliances  $C_{au}$ , while the Min AP is significantly influenced by the upper body arterial resistance  $R_{aup}$ .

Results for the time-averaged Sobol sensitivity indices are presented in Figure 22(b). It shows that the pressure within one cardiac cycle is most impacted by the time of maximum left ventricle elastance  $T_s$ . The time-averaged sensitivity indices for the left ventricle volume indicates that  $E_m$  is an important parameter for this quantity. It is important to note that  $C_{au}$  and  $C_{vu}$  have some contribution to the volume time series. Differently from the time-averaged

sensitivity indices, Figure 22(c) shows the Sobol indices as a function of time for the last cardiac cycle. One can observe that  $T_r$  and  $T_s$  are significant parameters during the systole for the pressure, whereas during diastole,  $E_m$  has high sensitivity values. For the volume, one can observe that the maximum elastance  $E_M$  is the dominant parameter during systole and beginning of diastole (for  $t \leq 0.3$  seconds). It is also important to note from panels (b) and (c) that some higher interaction between  $T_s$  and  $T_r$  occur for  $0.2 \leq t \leq 0.4$  seconds, as can be seen from total Sobol indices.

Figure 22 – Sensitivity analysis for the 5-compartment model. (a) Sobol’s indices; (b) time averaged Sobol’s indices  $TAS_i$  and  $TAS_{T,i}$  for left heart pressure and volume; and (c) time series for Sobol’s indices of pressure and volume.



Source: Elaborated by the author.

## 4.2 ANALYSIS OF THREE-COMPARTMENT MODEL

To perform an UQ and SA analysis of the 3-compartment model we define the set of uncertain parameters, as in the 5-compartment model, considering the parameters related to the elastance function, the resistances and the compliances as uncertain inputs:

$$\mathbf{Z}_3 = \{R_p, R_{mv}, R_{av}, C_a, C_v, E_M, E_m, T_s, T_r\}. \quad (4.2)$$

Here, we also set all parameters with a normal distribution with a coefficient of variation of 20% around their baseline values (from Table 6). The polynomial expansion in Equation (2.14)

was constructed with the same configurations used for the 5-compartment model, which also yielded a good convergence. Table 12 shows the determination coefficient computed for different combinations of  $p$  and  $m$ . Further increasing the polynomial degree or the multiplicative factor increases the accuracy as expected, but results in a significant increase in computational time which does not seem to pay off.

Table 12 – LOO accuracy for each QoI for the 3-compartment model.

Factor $m$	Order $p$	Samples $N_s$	$Q^2$					
			ESV	EDV	SV	EF	MaxAP	MinAP
1	1	10	0.6899	0.5719	0.8820	0.9990	0.9283	0.7303
2	1	20	0.8545	0.7237	0.8258	0.9996	0.7050	0.9327
3	1	30	0.9321	0.7963	0.8408	0.9997	0.8813	0.9061
4	1	40	0.9052	0.8563	0.8895	0.9996	0.8911	0.9162
1	2	55	0.8113	0.9485	0.8628	0.9995	0.6723	0.8693
2	2	110	0.9615	0.9524	0.9569	0.9999	0.9546	0.9672
3	2	165	0.9672	0.9456	0.9619	0.9999	0.9501	0.9717
<b>4</b>	<b>2</b>	<b>220</b>	<b>0.9671</b>	<b>0.9514</b>	<b>0.9604</b>	<b>0.9999</b>	<b>0.9562</b>	<b>0.9718</b>
1	3	220	0.9233	0.8784	0.9145	0.9998	0.9626	0.9520
2	3	440	0.9898	0.9868	0.9858	0.9999	0.9839	0.9902
3	3	660	0.9860	0.9883	0.9781	1.0000	0.9864	0.9878
4	3	880	0.9924	0.9890	0.9912	1.0000	0.9920	0.9930

Source: Elaborated by the author.

#### 4.2.1 UQ and SA results

Table 13 shows the uncertainty metrics calculated for the output quantities, while Figure 23 shows the left heart volume and pressure in time. The QoIs maintained their mean values and slightly increased their coefficient of variation in comparison to the 5-compartment model. The ESV was the output with the largest variation, achieving  $CoV=24\%$ .

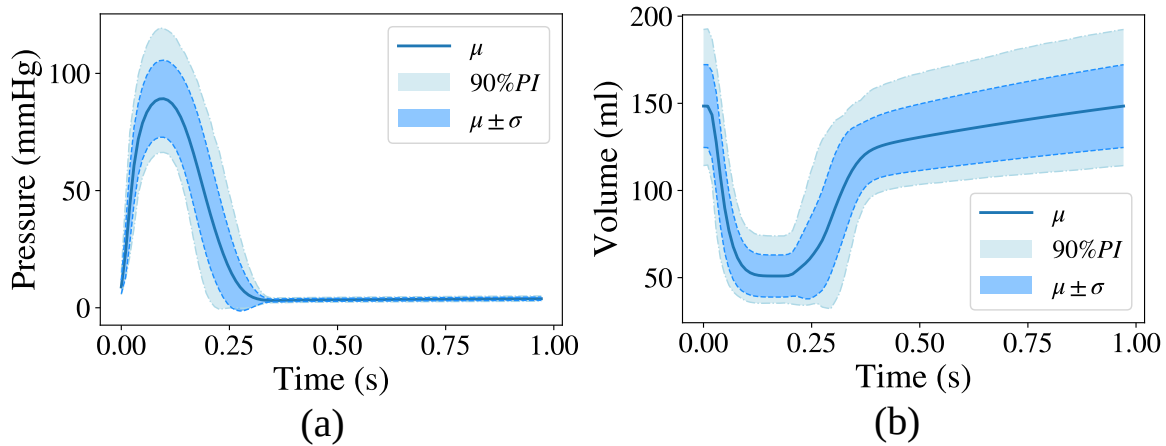
Table 13 – Uncertainty measures of each QoI for the 3-compartment model.

QoI	$\mu[Y]$	$\sigma[Y]$	$CoV[Y]$	90% PI
ESV [ml]	50.93	12.07	0.24	[35.34, 73.93]
EDV [ml]	148.42	23.75	0.16	[114.29, 192.36]
SV [ml]	97.50	18.56	0.19	[71.40, 132.13]
EF [-]	0.66	0.06	0.09	[0.55, 0.75]
MaxAP [mmHg]	90.53	16.53	0.18	[67.88, 120.61]
MinAP [mmHg]	53.77	10.45	0.19	[36.36, 70.15]

Source: Elaborated by the author.

The same behaviour of the results for the 5-compartment occurs in terms of the probability densities of the QoIs and, therefore, are not presented here. Results for the Sobol sensitivity indices are depicted in Figure 24(a). Maximum elastance  $E_M$  is the crucial parameter for the ESV

Figure 23 – Uncertainty propagation in the 3-compartment model for left ventricular pressure and volume; (a) pressure; (b) volume.



Source: Elaborated by the author.

and EF, EDV is more impacted by the minimum elastance  $E_m$ , whereas SV is more influenced by  $R_p$ . The MaxAP and MinAP are significantly influenced by the arterial compliance  $C_a$  and peripheral arteries resistance  $R_p$ , respectively.

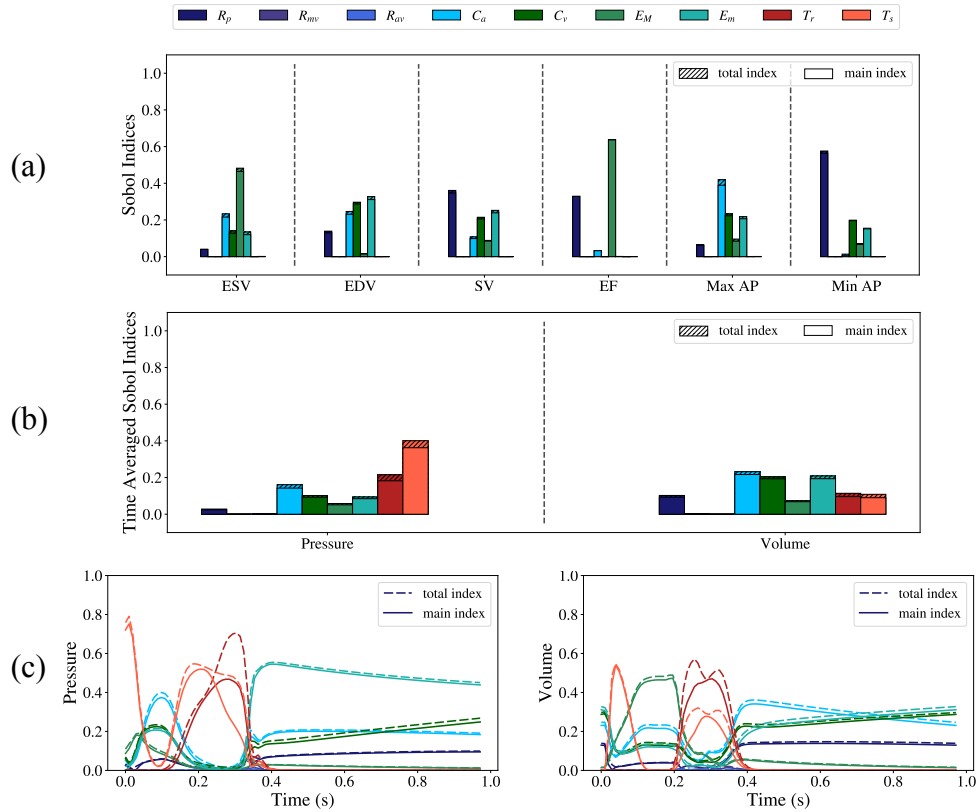
Results for the time averaged sensitivity indices are shown in Figure 24(b), where the same behaviour as in the five-compartment model can be observed here, that is,  $T_s$  has a high contribution to the pressure time series, whereas the set of parameters formed by  $C_a$  and  $E_m$  impact the volume time series. Figure 24(c) shows the Sobol indices as a function of time for the last cardiac cycle. For the volume time series, similarly to the five-compartment model, the maximum elastance  $E_M$  plays a significant role during systole and beginning of diastole. The timings at which maximum and minimum elastances occur ( $T_s$  and  $T_r$ , respectively) also contribute to the pressure and volume series.

### 4.3 ANALYSIS OF THE COUPLED MODEL

Given the complexity and computational demand of the coupled model, and the fact that to build the gPC surrogate model it is necessary to run the model multiple times, we used a reduced set of uncertain parameters to avoid an excessive computational cost. The coupled model is the result of coupling the: (i) 3-compartment circulatory model, (ii) continuum mechanics (or FE) model, and (iii) active stress model.

Considering the previous simulations results and the SA performed, we considered the 3-compartments model can provide a similar response in terms of LV hemodynamics compared to the 5-compartments model. For the choice of the uncertain input parameters, we chose the most influential parameters of the LP model simulations, which are the vessels compliances and the peripheral resistance ( $C_a$ ,  $C_v$  and  $R_p$ , respectively). Although the SA revealed that  $E_M$

Figure 24 – Sensitivity analysis for the 3-compartment model. (a) Sobol's indices; (b) time averaged Sobol's indices  $TAS_i$  and  $TAS_{T,i}$  for left heart pressure and volume; and (c) time series for Sobol's indices of pressure and volume.



Source: Elaborated by the author.

is a key parameter for EF, SV, and ESV, the elastance function is not present in the coupled model, which derives its elastance from the continuum mechanics model (see Figures 11 and 16). Consequently, the elastance parameters ( $E_M$ ,  $E_m$ ,  $T_r$ , and  $T_s$ ) were not considered in this study of the coupled model.

We also considered the parameters from the active stress curve (Section 3.3.2) in this study, since they have a direct effect on the duration and rise of the active stress curve, which can have a significant impact on the dynamics of systole and diastole. They are the maximum active stress value, the twitch rise constant and the twitch duration increase ( $T_{ref}$ ,  $\tau_r$  and  $b$ , respectively).

Then, for UQ and SA of the coupled model the following input parameters were considered:

$$\mathbf{Z}_{coupled} = \{C_a, C_v, R_p, T_{ref}, \tau_r, b\}. \quad (4.3)$$

We set all parameters with a normal distribution and 5% of variation around their baseline values (Table 8). The choice of a 5% of variation is mainly because greater variations would lead to non-physiological responses. To construct the polynomial expansion, we chose a polynomial

order  $p = 2$  and a multiplicative factor  $m = 3$ . With this number of samples we reached a reasonable convergence for almost all QoIs (see Table 14), while the computational demand could remain practicable.

The computational cost of the forward solution of the coupled model is considerably higher than that of the circulatory models. Therefore, a detailed study for the appropriate choice for the polynomial order and multiplicative factor for the coupled model, was not considered. Instead, we simply assumed the same setting used for the previous models could be applied to obtain a reasonable accuracy.

#### 4.3.1 UQ and SA results

The uncertainty metrics calculated are shown in Table 14 and in Figure 25 they are depicted for the left ventricle pressure and volume time series. The mean values are considerably different from those obtained for the uncoupled LP models, with the only exception being the EF which resulted in a value within the normal physiological range. One can also observe that the variation propagated is significantly low for most of the QoIs when compared to the results for the LP models, even if we consider that the inputs are subjected to only 5% of variation. The only exception is the ESV which presented the largest variation in terms of the coefficient of variation. For this case it is important to observe that the effects of the uncertainties in the left ventricular pressure and volume are mainly concentrated in the beginning of diastole, as shown in Figures 25 and 26.

Table 14 – Uncertainty measures of each QoI for the coupled model.

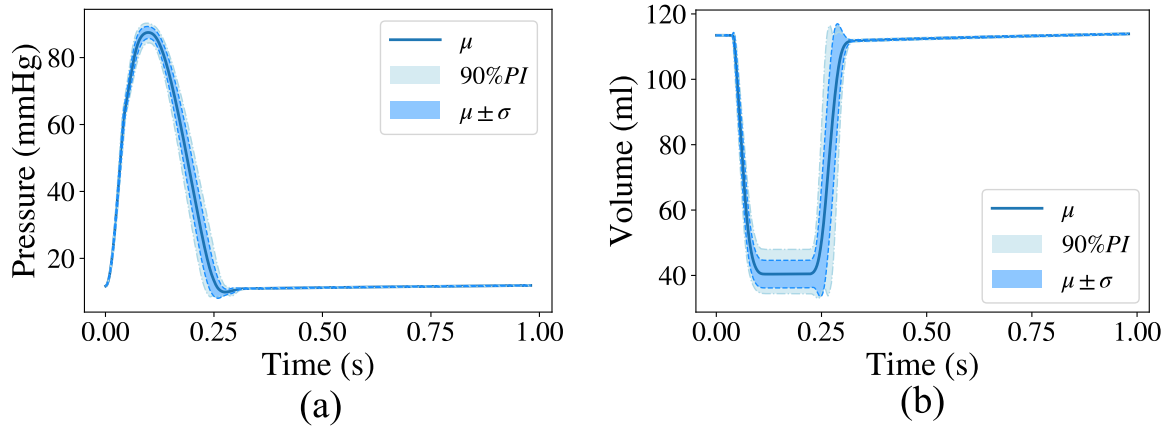
QoI	$\mu[Y]$	$\sigma[Y]$	$CoV[Y]$	90% PI	$Q^2$
ESV [ml]	40.39	4.22	0.10	[34.43, 47.94]	0.5399
EDV [ml]	113.89	0.17	0.001	[113.62, 114.18]	0.9867
SV [ml]	73.51	4.14	0.05	[66.18, 79.37]	0.5512
EF [-]	0.64	4.00	0.06	[0.58, 0.70]	0.9960
MaxAP [mmHg]	87.46	1.77	0.02	[84.36, 90.25]	0.8267
MinAP [mmHg]	57.37	1.78	0.03	[54.23, 60.14]	0.8833

Source: Elaborated by the author.

Figure 27 shows the probability density for the QoIs. The ranges given by (74) are not shown, since there is very little variability for most of the QoIs. In particular, we note that EF and ESV are within the ranges given by (74).

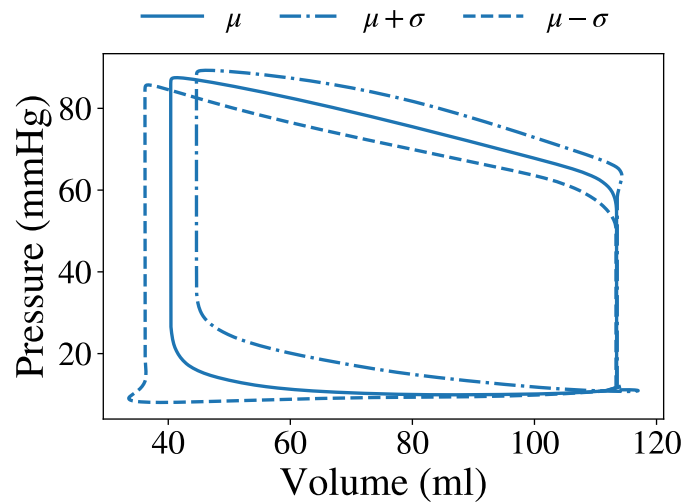
In Figure 28(a) the Sobol's sensitivity indices for the QoIs are depicted. ESV, SV, EF and Max AP are greatly impacted by the reference maximum stress value  $T_{ref}$ , while EDV and Min AP are more influenced by the peripheral resistance  $R_p$ . The time averaged Sobol indices reveal that the LV pressure and volume are more impacted by the twitch duration increase parameter  $b$ , as shown in Figure 28(b). In Figure 28(c) the Sobol's indices are depicted as a function of

Figure 25 – Uncertainty propagation in the coupled model for left ventricular pressure and volume; (a) pressure; (b) volume.



Source: Elaborated by the author.

Figure 26 – Uncertainty propagation for left ventricular pressure and volume loop in the coupled model.



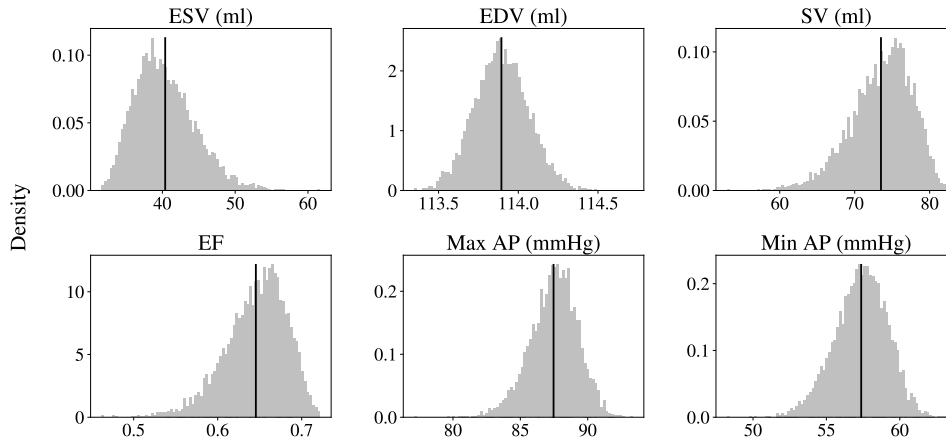
Source: Elaborated by the author.

time, and it is possible to observe the influence of  $b$  and  $T_{ref}$  during a considerable time interval. Lastly, one can see that very little discrepancy between the main and total indices occur for this model, indicating there is no significant higher order interaction between the parameters considered in this analysis.

#### 4.4 DISCUSSION

In this work we performed an UQ and SA analysis for LP models of the systemic circulation, as well as, with a coupled LP+FE model, which helped us find the most influential

Figure 27 – Evaluated distribution of each scalar QoIs for the coupled model.  
The thick black line is the mean value obtained with the UQ.



Source: Elaborated by the author.

uncertain inputs when measuring important quantities of clinical interest. In the following, we discuss the findings and limitations of this work, and also related work from the literature.

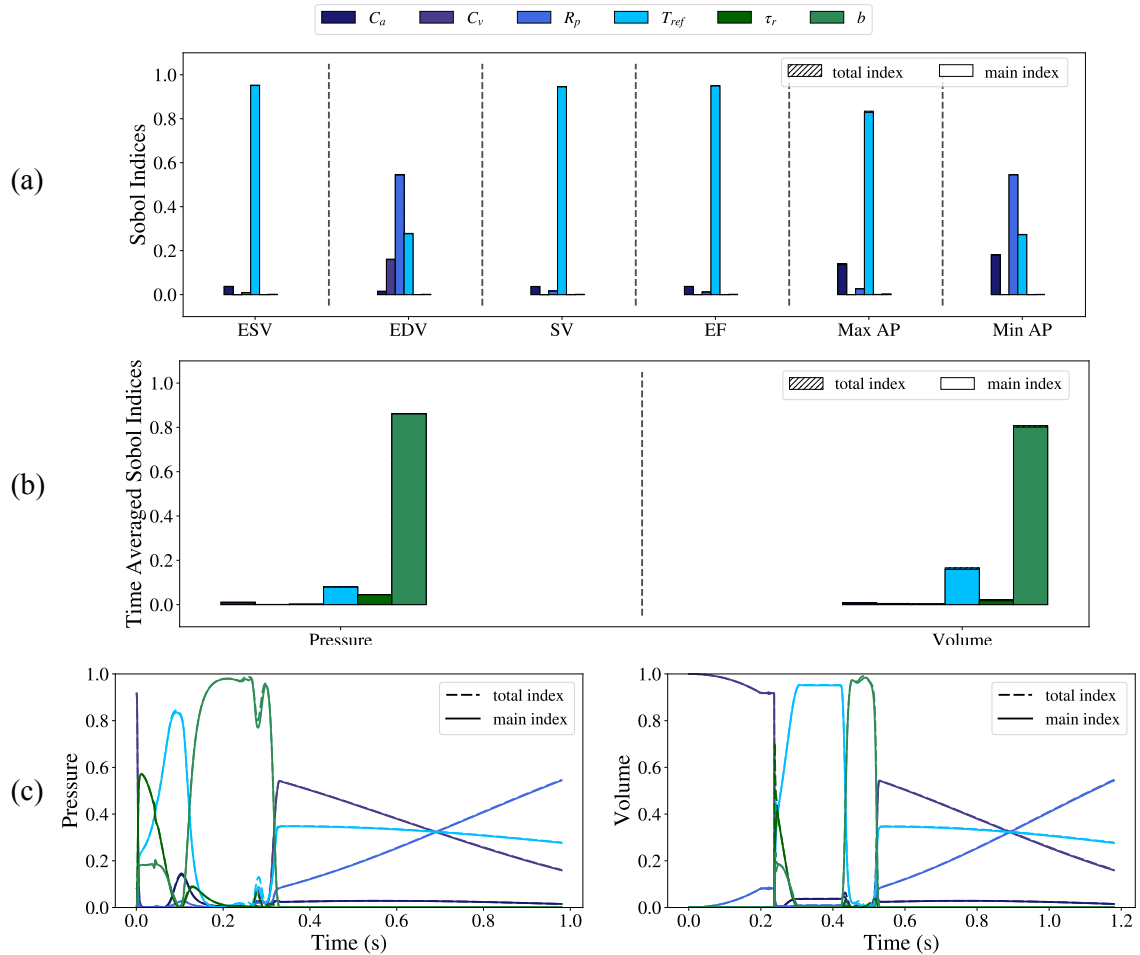
#### 4.4.1 Lumped parameter models

The LP models (5-compartment and 3-compartment) were subjected to an UQ and SA study with a CoV=20% for the uncertain inputs. The propagated uncertainty, for most of the QoIs, was lower than the variability of the inputs, except for the ESV which presented a 24% of variation. For the non-scalar QoIs, we observed that the left heart pressure showed the highest values of uncertainty around the end of systole, while the volume showed increasingly higher variability of diastole.

The sensitivity analysis of the 5-compartment model revealed that  $E_M$ ,  $E_m$ ,  $R_{aup}$ , and  $C_{au}$  are the most sensitive uncertain inputs for the chosen QoIs. The time-averaged Sobol indices indicated that parameters for the time at which maximum and minimum elastances occur  $T_s$  and  $T_r$ , respectively, are significant for pressure and volume time series. In general, the results of SA for the 3-compartment model were very similar to the one for the 5-compartment model. It revealed that  $E_M$ ,  $E_m$ ,  $R_p$ , and  $C_a$  are the inputs that most influence the variance of the outputs. Small differences were observed for SV and EF, where the  $R_p$  parameter appeared with higher sensitivity and  $E_m$  with lower when compared to their counterparts in the 5-compartment model. The results indicated that  $T_s$  and  $T_r$  have high values for time-averaged Sobol sensitivity indices.

With this analysis, we identified the most influential uncertain inputs and non-influential ones, which could be fixed to the literature or population-based values. For instance, in the 3-compartment model,  $R_{mv}$  and  $R_{av}$  could be fixed at their baseline values, due to their small

Figure 28 – Sensitivity analysis for the coupled model. (a) Sobol’s indices; (b) time averaged Sobol’s indices  $TAS_i$  and  $TAS_{T,i}$  for left heart pressure and volume; and (c) time series for Sobol’s indices of pressure and volume.



Source: Elaborated by the author.

sensitivity values for all physiological QoIs considered in this work. Whereas, due to high sensitivity values of  $E_M$ ,  $E_m$ ,  $R_p$ , and  $C_a$ , these parameters should be calibrated accurately since, for the QoIs analyzed in this work, they are highly influential. To summarize, the results for the 3-compartment model suggested that, at least for the quantities of interest and simulations performed in this work, the model retained the key characteristics and responses of the 5-compartment model.

#### 4.4.1.1 Model reduction

Model simplification could usually lead to less accurate or detailed predictions than a complex model. In contrast, calibrating a complex model is very difficult, and quite often, simplified models are better adjusted to patient-specific data (75).

In Section 3.2.2, we presented a possible reduction or simplification of the 5-compartment model to a 3-compartment model, which was then explored using UQ and SA. We observed that the reduced model maintained the quality of the predictions for LV hemodynamics. Also, the UQ studies showed that the range of uncertainty propagated in both models is very similar. Therefore, for the output quantities considered here, mainly related to LV function, the same insights provided by the 5-compartment model analysis could be achieved by the 3-compartment model.

The SA of the 5-compartment model showed that the parameters of the lower body, such as  $R_{al}$ ,  $R_{vl}$ , and  $C_{vl}$ , have minimal impact on the LV hemodynamics outputs under consideration. This fact corroborates with the results obtained in which the 3-compartment model obtained a similar response to the 5-compartment model in the simulations performed.

However, it is essential to remark that this reduced model neglected the distinction between the upper and lower parts of the body since they were merged to reduce the number of compartments. Therefore, the reduced 3-compartment model could not be appropriate for simulating sudden hemodynamics shifts such as postural changes or a localized variation in vascular properties between upper and lower parts of the body, such as the cardiovascular regulation during HUT (25).

#### 4.4.2 Coupled model

Since the 3-compartment model response was suitable for left ventricle hemodynamics, it was used to perform a coupled multi-scale simulation of a full cardiac cycle. In this scenario, the LP model was coupled to a FE model of the left ventricle mechanics. It is important to remark that the coupled model was not adjusted to reproduce the same LV hemodynamics of the uncoupled LP models, which would require a detailed calibration of the left ventricle FE model.

The coupled model was analyzed with parameters that consider the most influential circulatory parameters and the active stress parameters that can impact the dynamics of systole and diastole. With this, the set of parameters subjected to a CoV=5% produced very few uncertainties to almost all scalar QoIs, in special EDV showed a small CoV=1%. The exception was the ESV, which showed a CoV=10%, which is twice the variation present in the inputs. These results show that, when considering this particular set of uncertain inputs, although the coupled model is consistent in measuring most of the QoIs, it propagates a considerable amount of uncertainty to ESV. These facts are observed in the time series results since the highest values of uncertainty are concentrated at the end of systole and the beginning of diastole interval for both the LV pressure and volume.

The sensitivity analysis showed that quantities related to the end of diastole, that is EDV and Min AP, are the least influenced by the uncertainties in the inputs. They are also the most influenced by circulatory parameters, specially the peripheral resistance  $R_p$  and the

vessels compliances  $C_a$  and  $C_v$ . Specifically,  $C_a$  is more influential when measuring the Min AP, whereas  $C_v$  is more influential when measuring the EDV, and  $R_p$  is the most influential for both the QoIs. For the other QoIs,  $T_{ref}$  is greatly influential, while  $\tau_r$  and  $b$  have negligible impact. On the other hand, when we consider the time series QoIs,  $b$  is the most influential parameter, and  $T_{ref}$  and  $\tau_r$  have very little impact, while the circulatory parameters have negligible impact on average.

Despite this fact, the UQ and SA analyses of the coupled model were useful to reveal important information about the model. For instance, the sensitivity analysis showed that the maximum value of the active stress  $T_{ref}$  is the parameter which most affects ESV, SV, EF, and MaxAP. This finding is consistent with the literature (76), where it is reported that the  $T_{ref}$  parameter represents different levels of contractility, which affects the pressure and volume of the LV cavity.

The simulation of a cardiac cycle with the coupled model produced qualitative results similar to the simulation made with the LP models. Some physiological outputs showed values within the normal range (EDV and EF), while others were relatively a little lower than reported typical values from the literature. This fact indicates that for a detailed analysis, the parameters have to be adequately calibrated. To summarize, in the analysis of the coupled model, we found out that the parameters regarding the active stress curve (which are also related to contractility) are the most influential and, therefore, should be measured or calibrated more accurately.

Regarding the choice of the uncertain parameters considered for the analysis ( $\mathbf{Z}_{coupled}$ ), we left out many parameters from the FE LV mainly to ease the analysis, since we wanted the analysis to be focused and not too computationally burdensome. We also remark that other properties of cardiac mechanics were explored in the literature, such as the parameters related to the constitutive mechanics and the active stress (15, 4, 42, 43).

#### 4.4.3 Related work

Here, we discuss related work of the literature and compare them to the present study in terms of our methods and findings. In (77) a mathematical model based on experimental data to investigate how parameters describing the heart and the arterial system contribute to the systolic and diastolic pressures and stroke volume was presented. Dimensional and sensitivity analysis were used in their work to characterize the role of the parameters. In particular, they showed that the minimum elastance and venous pressures (denoted as  $E_{min}$  and  $P_v$  in their work) determine filling and end-diastolic volume. Our SA results agree with their findings since the minimum elastance  $E_{min}$  and the venous compliance  $C_{vu}$  for the 5-compartment model (or  $C_v$  for the 3-compartment model), revealed to be essential parameters for EDV and SV.

Another feature identified by the SA study was the relevance of maximum elastance  $E_M$  parameter, representing a particular state of contractility (77). The maximum elastance

$E_M$  is known (78, 79, 59) to be determinant for the left ventricular EF. The Sobol sensitivity analyses performed in this work for the two lumped parameter models confirmed this behavior, where high values were obtained for the sensitivity of EF concerning  $E_M$ . Simple mathematical equations could be used to explain the relation between  $E_M$  and EF or other outputs, as shown in (79). However, this could be a difficult task for nonlinear time-dependent or more complex models, as is the case for coupled PDEs, such as those studied in this work or reported in the literature (15, 75). These results highlight the efficacy and viability of the Sobol SA method for identifying the essential features that complex physiological models should be able to describe.

Lumped parameter models of the cardiovascular system have been studied in the context of uncertainty quantification and sensitivity analysis in the literature (36, 80, 31, 32, 33). In particular, (32) presented a practical identifiability approach based on sensitivity analysis and uncertainty quantification for a lumped parameter cardiovascular model calibrated with experimental rat data. The analysis was based on the Markov-Chain Monte-Carlo (MCMC) method for model calibration and uncertainty propagation. For sensitivity analysis, a local method based on partial derivatives was employed. First, we note that the results of the present work are in good agreement with the findings of the local SA methods used in (32), in the sense that both identified  $E_M$ ,  $E_m$ ,  $T_r$ , and  $T_s$  as critical parameters of the model. However, we remark that the Sobol indices and its time-averaged variants used in this work revealed that compliance parameters, such as  $C_{au}$  (for the five-compartment model) and  $C_a$  (for the three-compartment model), also contribute significantly to the variability of pressure and volume in time. Besides the advantages of global SA analysis over local techniques discussed in Section 2.2, we remark that the variance-based Sobol approach can provide information on how the input parameters affect essential QoIs, rather than quantifying the sensitivity with respect to the residual (32). With the approach used in this work, one can gain insight into the model or verify that it can reproduce known physiological relations.

## 5 CONCLUSION

In the present work, global uncertainty quantification and sensitivity analysis were used to study mathematical models of the cardiovascular system. Two lumped parameter models and a coupled model were analyzed. We presented an efficient approach based on polynomial chaos, which allowed us to assess the propagation of uncertainties from parameters to the model predictions and identify the essential parameters using variance-based Sobol sensitivity analysis. Besides, a possible reduction of the 5-compartment model was presented and evaluated in terms of its response to LV hemodynamics.

Uncertainty quantification results consistently indicated, for all the models studied, that ESV is the quantity of interest most impacted by the uncertainties in the input parameters. The other QoIs presented levels of variation below the one considered for the inputs. Sensitivity analysis of the lumped parameter models indicated that, in general, parameters related to the elastance of the LV ( $E_M$ ,  $E_m$ ,  $T_r$ , and  $T_s$ ) are the most influential for the QoIs. The SA results for the 5-compartment model, indicating that lower body parameters have insignificant effects on LV hemodynamics, explains why the reduced 3-compartment model had a similar response as the complete model. Additionally, the SA for the coupled model revealed that the active stress parameters are very influential, especially the maximum active stress value for the scalar QoIs, while the twitch duration increase is very influential for left ventricular pressure and volume time series.

In summary, we have shown the viability of using the polynomial chaos method and Sobol indices for UQ and SA studies of lumped parameters and coupled LP/FE mechanics of the left ventricle. The methods have shown to be efficient and reliable, considering that the SA captured known physiological relations. Also, SA has shown to be an essential tool during the reduction of the LP model, which in turn demonstrated to be as good as a more complex model for describing relevant left ventricular function biomarkers.

### 5.1 LIMITATIONS AND FUTURE WORKS

This work has some limitations which are worth mentioning. We equally applied a 20% variation to the baseline values of the model parameters. The assumed 20% variation could not be equally relevant to all parameters. Also, one further investigation regarding the assumptions adopted in this work would be to explore if the input parameters are indeed independent and identically distributed, as assumed here for the application of the gPC.

Additionally, the values obtained for the systolic and diastolic pressure in the simulations are a little below the physiological values. However, as stated before, the baseline values for the parameters were taken from (32), and no procedure to calibrate these outputs of the model was considered here. With these limitations in mind, one natural extension of the present work

is to calibrate the model using experimental data. Ideally, that could be performed using an inverse uncertainty quantification technique such as the Markov Chain Monte Carlo (MCMC) method (81) or the Sequential Monte Carlo (SMC) to estimate the distribution of the input parameters.

Also, regarding the coupled model, a complete study of the active stress model could be done by considering more of its uncertain parameters and their interactions in the analysis. It is worth noting that the active stress model used (26) is a rather simple model. Thus, it would also be interesting to consider using a more realistic active stress model (70) and to analyze the effects of uncertainties in its parameters when simulating the coupled model.

## REFERENCES

- 1 WHO. *Cardiovascular Diseases (CVDs)*. World Health Organization. Disponível em: <[https://www.who.int/news-room/fact-sheets/detail/cardiovascular-diseases-\(cvds\)](https://www.who.int/news-room/fact-sheets/detail/cardiovascular-diseases-(cvds))>. Acesso em: 15 jan 2020.
- 2 STEVENS, B. et al. Os custos das doenças cardíacas no brasil. *Arquivos Brasileiros de Cardiologia*, SciELO Brasil, v. 111, n. 1, p. 29–36, 2018.
- 3 ECK, V. G. et al. A guide to uncertainty quantification and sensitivity analysis for cardiovascular applications. *International journal for numerical methods in biomedical engineering*, Wiley Online Library, v. 32, n. 8, p. e02755, 2016.
- 4 LEVRERO-FLORENCIO, F. et al. Sensitivity analysis of a strongly-coupled human-based electromechanical cardiac model: Effect of mechanical parameters on physiologically relevant biomarkers. *Computer Methods in Applied Mechanics and Engineering*, Elsevier, v. 361, p. 112762, 2020.
- 5 NIEDERER, S. A.; CAMPBELL, K. S.; CAMPBELL, S. G. A short history of the development of mathematical models of cardiac mechanics. *Journal of molecular and cellular cardiology*, Elsevier, v. 127, p. 11–19, 2019.
- 6 SEVERI, S.; RODRIGUEZ, B.; ZAZA, A. *Computational cardiac electrophysiology is ready for prime time*. [S.l.]: Oxford University Press, 2014.
- 7 BESSONOV, N. et al. Methods of blood flow modelling. *Mathematical modelling of natural phenomena*, EDP Sciences, v. 11, n. 1, p. 1–25, 2016.
- 8 NIEDERER, S. A.; LUMENS, J.; TRAYANOVA, N. A. Computational models in cardiology. *Nature Reviews Cardiology*, Nature Publishing Group, v. 16, n. 2, p. 100–111, 2019.
- 9 TRAYANOVA, N. A. Whole-heart modeling: applications to cardiac electrophysiology and electromechanics. *Circulation research*, Am Heart Assoc, v. 108, n. 1, p. 113–128, 2011.
- 10 VIGNON-CLEMENTEL, I. E. et al. Outflow boundary conditions for three-dimensional finite element modeling of blood flow and pressure in arteries. *Computer methods in applied mechanics and engineering*, Elsevier, v. 195, n. 29-32, p. 3776–3796, 2006.
- 11 KIM, H. et al. Patient-specific modeling of blood flow and pressure in human coronary arteries. *Annals of biomedical engineering*, Springer, v. 38, n. 10, p. 3195–3209, 2010.
- 12 LEE, L. C. et al. Analysis of patient-specific surgical ventricular restoration: importance of an ellipsoidal left ventricular geometry for diastolic and systolic function. *Journal of applied physiology*, American Physiological Society Bethesda, MD, v. 115, n. 1, p. 136–144, 2013.
- 13 OKADA, J.-i. et al. Multi-scale, tailor-made heart simulation can predict the effect of cardiac resynchronization therapy. *Journal of molecular and cellular cardiology*, Elsevier, v. 108, p. 17–23, 2017.
- 14 OLIVEIRA, R. S. et al. Ectopic beats arise from micro-reentries near infarct regions in simulations of a patient-specific heart model. *Scientific reports*, Nature Publishing Group, v. 8, n. 1, p. 1–14, 2018.

- 15 CAMPOS, J. O. et al. Effects of left ventricle wall thickness uncertainties on cardiac mechanics. *Biomechanics and modeling in mechanobiology*, Springer, v. 18, n. 5, p. 1415–1427, 2019.
- 16 JIE, X.; TRAYANOVA, N. A. Mechanisms for initiation of reentry in acute regional ischemia phase 1b. *Heart Rhythm*, Elsevier, v. 7, n. 3, p. 379–386, 2010.
- 17 NOBLE, D. et al. The role of sodium-calcium exchange during the cardiac action potential a. *Annals of the New York Academy of Sciences*, Wiley Online Library, v. 639, n. 1, p. 334–353, 1991.
- 18 SHI, Y.; LAWFORDE, P.; HOSE, R. Review of zero-d and 1-d models of blood flow in the cardiovascular system. *Biomedical engineering online*, Springer, v. 10, n. 1, p. 33, 2011.
- 19 WESTERHOF, N.; LANKHAAR, J.-W.; WESTERHOF, B. E. The arterial windkessel. *Medical & biological engineering & computing*, Springer, v. 47, n. 2, p. 131–141, 2009.
- 20 WATANABE, H. et al. Multiphysics simulation of left ventricular filling dynamics using fluid-structure interaction finite element method. *Biophysical journal*, Elsevier, v. 87, n. 3, p. 2074–2085, 2004.
- 21 LIANG, F.; LIU, H. A closed-loop lumped parameter computational model for human cardiovascular system. *JSME International Journal Series C Mechanical Systems, Machine Elements and Manufacturing*, The Japan Society of Mechanical Engineers, v. 48, n. 4, p. 484–493, 2005.
- 22 DUANMU, Z. et al. A patient-specific lumped-parameter model of coronary circulation. *Scientific reports*, Nature Publishing Group, v. 8, n. 1, p. 1–10, 2018.
- 23 LI, J. K. *The arterial circulation: physical principles and clinical applications*. [S.l.]: Springer Science & Business Media, 2000.
- 24 THROCKMORTON, A. L. et al. Mechanical cavopulmonary assistance of a patient-specific fontan physiology: numerical simulations, lumped parameter modeling, and suction experiments. *Artificial organs*, Wiley Online Library, v. 35, n. 11, p. 1036–1047, 2011.
- 25 WILLIAMS, N. D. et al. Patient-specific modelling of head-up tilt. *Mathematical Medicine and Biology: A Journal of the IMA*, OUP, v. 31, n. 4, p. 365–392, 2014.
- 26 BOVENDEERD, P. H.; KROON, W.; DELHAAS, T. Determinants of left ventricular shear strain. *American Journal of Physiology-Heart and Circulatory Physiology*, American Physiological Society, v. 297, n. 3, p. H1058–H1068, 2009.
- 27 KAYVANPOUR, E. et al. Towards personalized cardiology: multi-scale modeling of the failing heart. *PLoS One*, Public Library of Science, v. 10, n. 7, p. e0134869, 2015.
- 28 ECK, V.; STURDY, J.; HELLEVIK, L. Effects of arterial wall models and measurement uncertainties on cardiovascular model predictions. *Journal of biomechanics*, Elsevier, v. 50, p. 188–194, 2017.
- 29 ELLWEIN, L. M. et al. *Cardiovascular and respiratory regulation, modeling and parameter estimation*. Tese (Doutorado), 2008.

- 30 ELLWEIN, L. M. et al. Sensitivity analysis and model assessment: mathematical models for arterial blood flow and blood pressure. *Cardiovascular Engineering*, Springer, v. 8, n. 2, p. 94–108, 2008.
- 31 HUBERTS, W. et al. Applicability of the polynomial chaos expansion method for personalization of a cardiovascular pulse wave propagation model. *International journal for numerical methods in biomedical engineering*, Wiley Online Library, v. 30, n. 12, p. 1679–1704, 2014.
- 32 MARQUIS, A. D. et al. Practical identifiability and uncertainty quantification of a pulsatile cardiovascular model. *Mathematical biosciences*, Elsevier, v. 304, p. 9–24, 2018.
- 33 WILLIAMS, N. D. et al. Cardiovascular dynamics during head-up tilt assessed via pulsatile and non-pulsatile models. *Journal of mathematical biology*, Springer, v. 79, n. 3, p. 987–1014, 2019.
- 34 SALTELLI, A. et al. *Global sensitivity analysis: the primer*. [S.l.]: John Wiley & Sons, 2008.
- 35 XIU, D. *Numerical methods for stochastic computations: a spectral method approach*. [S.l.]: Princeton university press, 2010.
- 36 DONDERS, W. et al. Personalization of models with many model parameters: an efficient sensitivity analysis approach. *International journal for numerical methods in biomedical engineering*, Wiley Online Library, v. 31, n. 10, 2015.
- 37 WIENER, N. The homogeneous chaos. *American Journal of Mathematics*, JSTOR, v. 60, n. 4, p. 897–936, 1938.
- 38 XIU, D.; KARNIADAKIS, G. E. The wiener–askey polynomial chaos for stochastic differential equations. *SIAM journal on scientific computing*, SIAM, v. 24, n. 2, p. 619–644, 2002.
- 39 SCHIAVAZZI, D. E. et al. Patient-specific parameter estimation in single-ventricle lumped circulation models under uncertainty. *International journal for numerical methods in biomedical engineering*, Wiley Online Library, v. 33, n. 3, p. e02799, 2017.
- 40 HU, Z.; DU, D.; DU, Y. Generalized polynomial chaos-based uncertainty quantification and propagation in multi-scale modeling of cardiac electrophysiology. *Computers in biology and medicine*, Elsevier, v. 102, p. 57–74, 2018.
- 41 HURTADO, D. E.; CASTRO, S.; MADRID, P. Uncertainty quantification of 2 models of cardiac electromechanics. *International journal for numerical methods in biomedical engineering*, Wiley Online Library, v. 33, n. 12, p. e2894, 2017.
- 42 OSNES, H.; SUNDNES, J. Uncertainty analysis of ventricular mechanics using the probabilistic collocation method. *IEEE transactions on biomedical engineering*, IEEE, v. 59, n. 8, p. 2171–2179, 2012.
- 43 RODRÍGUEZ-CANTANO, R.; SUNDNES, J.; ROGNES, M. E. Uncertainty in cardiac myofiber orientation and stiffnesses dominate the variability of left ventricle deformation response. *International journal for numerical methods in biomedical engineering*, Wiley Online Library, v. 35, n. 5, p. e3178, 2019.

- 44 HUBERTS, W. et al. A sensitivity analysis of a personalized pulse wave propagation model for arteriovenous fistula surgery. part a: Identification of most influential model parameters. *Medical engineering & physics*, Elsevier, v. 35, n. 6, p. 810–826, 2013.
- 45 CHENG, C. P.; PARKER, D.; TAYLOR, C. A. Quantification of wall shear stress in large blood vessels using lagrangian interpolation functions with cine phase-contrast magnetic resonance imaging. *Annals of biomedical engineering*, Springer, v. 30, n. 8, p. 1020–1032, 2002.
- 46 TATANG, M. A. et al. An efficient method for parametric uncertainty analysis of numerical geophysical models. *Journal of Geophysical Research: Atmospheres*, Wiley Online Library, v. 102, n. D18, p. 21925–21932, 1997.
- 47 KAMINSKI, M. *The stochastic perturbation method for computational mechanics*. [S.l.]: John Wiley & Sons, 2013.
- 48 ZHANG, D. *Stochastic methods for flow in porous media: coping with uncertainties*. [S.l.]: Elsevier, 2001.
- 49 SOBOL, I. M. Global sensitivity indices for nonlinear mathematical models and their monte carlo estimates. *Mathematics and computers in simulation*, Elsevier, v. 55, n. 1-3, p. 271–280, 2001.
- 50 SUDRET, B. Global sensitivity analysis using polynomial chaos expansions. *Reliability engineering & system safety*, Elsevier, v. 93, n. 7, p. 964–979, 2008.
- 51 FEINBERG, J.; LANGTANGEN, H. P. Chaospy: An open source tool for designing methods of uncertainty quantification. *Journal of Computational Science*, Elsevier, v. 11, p. 46–57, 2015.
- 52 BLATMAN, G.; SUDRET, B. Efficient computation of global sensitivity indices using sparse polynomial chaos expansions. *Reliability Engineering & System Safety*, Elsevier, v. 95, n. 11, p. 1216–1229, 2010.
- 53 MARIK, P. E.; MONNET, X.; TEBOUL, J.-L. Hemodynamic parameters to guide fluid therapy. *Annals of intensive care*, Springer, v. 1, n. 1, p. 1, 2011.
- 54 HALL, J. E.; HALL, M. E. *Guyton and Hall textbook of medical physiology e-Book*. [S.l.]: Elsevier Health Sciences, 2016.
- 55 HOPPENSTEADT, F. C.; PESKIN, C. S. *Modeling and simulation in medicine and the life sciences*. [S.l.]: Springer Science & Business Media, 2012. v. 10.
- 56 KEENER, J. P.; SNEYD, J. *Mathematical physiology*. [S.l.]: Springer, 1998. v. 1.
- 57 KLABUNDE, R. *Cardiovascular physiology concepts*. [S.l.]: Lippincott Williams & Wilkins, 2011.
- 58 OTTESEN, J. T.; OLUFSEN, M. S.; LARSEN, J. K. *Applied mathematical models in human physiology*. [S.l.]: SIAM, 2004.
- 59 SAGAWA, K.; SUGA, H.; NAKAYAMA, K. Instantaneous pressure-volume ratio of the left ventricle versus instantaneous force-length relation of papillary muscle. *Cardiovascular system dynamics*, p. 99–105, 1978.

- 60 LEVEQUE, R. J. *Finite difference methods for ordinary and partial differential equations: steady-state and time-dependent problems*. [S.l.]: SIAM, 2007.
- 61 WANNER, G.; HAIRER, E. *Solving ordinary differential equations II*. [S.l.]: Springer Berlin Heidelberg, 1996.
- 62 JONES, E. et al. *SciPy: Open source scientific tools for Python, 2001*. 2001.
- 63 BONET, J.; WOOD, R. D. *Nonlinear continuum mechanics for finite element analysis*. [S.l.]: Cambridge university press, 1997.
- 64 CAMPOS, J. O. et al. Preconditioned augmented lagrangian formulation for nearly incompressible cardiac mechanics. *International journal for numerical methods in biomedical engineering*, Wiley Online Library, v. 34, n. 4, p. e2948, 2018.
- 65 COSTA, K. D.; HOLMES, J. W.; MCCULLOCH, A. D. Modelling cardiac mechanical properties in three dimensions. *Philosophical transactions of the Royal Society of London. Series A: Mathematical, physical and engineering sciences*, The Royal Society, v. 359, n. 1783, p. 1233–1250, 2001.
- 66 COSTA, K. D. et al. A three-dimensional finite element method for large elastic deformations of ventricular myocardium: Ii—prolate spheroidal coordinates. 1996.
- 67 GUCCIONE, J. M.; MCCULLOCH, A. D.; WALDMAN, L. Passive material properties of intact ventricular myocardium determined from a cylindrical model. 1991.
- 68 AMBROSI, D.; PEZZUTO, S. Active stress vs. active strain in mechanobiology: constitutive issues. *Journal of Elasticity*, Springer, v. 107, n. 2, p. 199–212, 2012.
- 69 KERCKHOFFS, R. et al. Homogeneity of cardiac contraction despite physiological asynchrony of depolarization: a model study. *Annals of biomedical engineering*, Springer, v. 31, n. 5, p. 536–547, 2003.
- 70 RICE, J. J. et al. Approximate model of cooperative activation and crossbridge cycling in cardiac muscle using ordinary differential equations. *Biophysical journal*, Elsevier, v. 95, n. 5, p. 2368–2390, 2008.
- 71 KERCKHOFFS, R. C. et al. Coupling of a 3d finite element model of cardiac ventricular mechanics to lumped systems models of the systemic and pulmonic circulation. *Annals of biomedical engineering*, Springer, v. 35, n. 1, p. 1–18, 2007.
- 72 ATKINSON, K. E. *An introduction to numerical analysis*. [S.l.]: John wiley & sons, 2008.
- 73 SAAD, Y. *Iterative methods for sparse linear systems*. [S.l.]: SIAM, 2003.
- 74 MACEIRA, A. et al. Normalized left ventricular systolic and diastolic function by steady state free precession cardiovascular magnetic resonance. *Journal of Cardiovascular Magnetic Resonance*, Taylor & Francis, v. 8, n. 3, p. 417–426, 2006.
- 75 EPSTEIN, S. et al. Reducing the number of parameters in 1d arterial blood flow modeling: less is more for patient-specific simulations. *American Journal of Physiology-Heart and Circulatory Physiology*, American Physiological Society Bethesda, MD, v. 309, n. 1, p. H222–H234, 2015.

- 76 KALLHOVD, S.; SUNDNES, J.; WALL, S. Sensitivity of stress and strain calculations to passive material parameters in cardiac mechanical models using unloaded geometries. *Computer methods in biomechanics and biomedical engineering*, Taylor & Francis, v. 22, n. 6, p. 664–675, 2019.
- 77 STERGIOPULOS, N.; MEISTER, J.-J.; WESTERHOF, N. Determinants of stroke volume and systolic and diastolic aortic pressure. *American Journal of Physiology-Heart and Circulatory Physiology*, v. 270, n. 6, p. H2050–H2059, 1996.
- 78 GARCÍA, M. I. M. et al. Determinants of left ventricular ejection fraction and a novel method to improve its assessment of myocardial contractility. *Annals of Intensive Care*, SpringerOpen, v. 9, n. 1, p. 1–10, 2019.
- 79 ROBOTHAM, J. L. et al. Ejection fraction revisited. *Anesthesiology: The Journal of the American Society of Anesthesiologists*, The American Society of Anesthesiologists, v. 74, n. 1, p. 172–183, 1991.
- 80 HEINEN, S. et al. A metamodeling approach for instant severity assessment and uncertainty quantification of iliac artery stenoses. *Journal of biomechanical engineering*, American Society of Mechanical Engineers Digital Collection, v. 142, n. 1, 2020.
- 81 GEYER, C. J. Practical markov chain monte carlo. *Statistical science*, JSTOR, p. 473–483, 1992.